3-23-2017

Cavity perturbation technique of 10 GHz cylindrical resonator for modeling RF/IR sensor radomes/windows

Marvin-Ray Arida

CAVITY PERTURBATION TECHNIQUE MODELING OF A 10-GHZ CYLINDRICAL RESONATOR FOR MEASURING DIELECTRIC PROPERTIES OF MATERIALS AT VERY HIGH TEMPERATURES

THESIS

Marvin-Ray Arida, Captain, USAF

AFIT-ENP-MS-17-M-086

DEPARTMENT OF THE AIR FORCE
AIR UNIVERSITY

AIR FORCE INSTITUTE OF TECHNOLOGY

Wright-Patterson Air Force Base, Ohio

AFIT-ENP-MS-17-M-086

CAVITY PERTURBATION TECHNIQUE MODELING OF A 10-GHZ CYLINDRICAL RESONATOR FOR MEASURING DIELECTRIC PROPERTIES OF MATERIALS AT VERY HIGH TEMPERATURES

THESIS

Presented to the Faculty

Department of Physics

Graduate School of Engineering and Management

Air Force Institute of Technology

Air University

Air Education and Training Command

in Partial Fulfillment of the Requirements for the

Degree of Master of Science in Optical Sciences and Engineering

Marvin-Ray Arida, B.S.E.E.

Captain, USAF

March 23, 2017

AFIT-ENP-MS-17-M-086

CAVITY PERTURBATION TECHNIQUE MODELING OF A 10-GHZ CYLINDRICAL RESONATOR FOR MEASURING DIELECTRIC PROPERTIES OF MATERIALS AT VERY HIGH TEMPERATURES

Marvin-Ray Arida, B.S.E.E.
Captain, USAF

Committee Membership:

Michael Marciniak, PhD
Chair

Augustine Urbas, PhD
Member

James Park, PhD
Member

Peter Collins, PhD
Member

Abstract

The dielectric properties of candidate materials for radomes or sensor windows on hypersonic vehicles, which can reach temperatures above 1,500° Celsius when traveling greater than Mach 5, are required. Although there has been recent scientific interest in the temperature dependence of the dielectric constant, little is known for temperatures near 1,500° Celsius and above. Current research utilizes large laboratory-sized furnaces to achieve these temperatures. This also requires large sample sizes, which are expensive; such expense is greatly multiplied when sweeping through hundreds of materials for research and development. In an effort to reduce these costs, this thesis modeled a 7.0 cm×2.295 cm×1.016 cm rectangular waveguide aperture-coupled to a cylindrical cavity designed to operate at a resonant frequency of 10GHz, and utilized the electromagnetic cavity-perturbation technique to optimize the research of small dielectric disk samples placed within that cavity. The objective was to model the much smaller system, produce an empirical relationship between the cavity resonance and the dielectric constant of the sample, and create a prototype of the design to validate the proof of concept. Such samples could then be laser heated to these very high temperatures. As a result, it was found that a disk of 150μm thickness with a small radius, positioned at the center of the resonant cavity, is a viable geometry to produce the sensitivity required for conducting dielectric measurements as a function of sample temperature.

Acknowledgments

I would like to express my sincere appreciation to my faculty advisor, Dr. Marciniak, for his guidance and support throughout the course of this thesis effort. The insight and experience was certainly appreciated. I would also like to thank my sponsor, Dr. Urbas, from the Air Force Research Laboratory for both the support and latitude provided to me during this endeavor. Thank you, Dr. Collins, for taking me on as a student at crunch time. Thank you to Dr. Park and Dr. Ku for their countless hours of assistance with the modeling and theory of my research. Lastly, and most importantly, I would like to thank my wife and our children for your continued love, patience, and support throughout my numerous absences and irregular work schedule during my tenure of the AFIT Masters' program. I most definitely could not have completed this arduous program without all of your support and I am much better off for it.

Marvin-Ray Arida

Table of Contents

Page

List of Figures

Figure Page

CAVITY PERTURBATION TECHNIQUE MODELING OF A 10-GHZ CYLINDRICAL RESONATOR FOR MEASURING DIELECTRIC PROPERTIES OF MATERIALS AT VERY HIGH TEMPERATURES

I. Introduction

1.1 Motivation

The motivation of this research is to create a novel approach to measuring dielectric properties of multi-spectral materials that will be used to create radar domes (radomes), the top of Figure 1.1, or sensor windows, the middle of Figure 1.1, that are sustainable in extreme environments. A radome is a structure that protects the sensor, but does not interfere with its operation [12]. The endstate was to analyze the correlation between permittivity and temperature by merging cavity perturbation with laser heating, where previous research has shown that as temperature increases, permittivities increase [13, 14]. This research initiates the first step towards this correlation by designing a cylindrical cavity, which can be measured at microwave frequencies. The frequencies of interest in the electromagnetic spectrum are the infrared and microwave ranges. This research provides emphasis on the microwave frequencies, but the infrared spectrum will be studied using beam deflection by another team of researchers, all with the goal of creating a common aperture for both spectra. The goal is to test materials heated to greater than $1,500^{\circ}$ Celsius. Such temperatures can be achieved by hypersonic vehicles, illustrated by the bottom of Figure 1.1, traveling at Mach 5 and above [15].

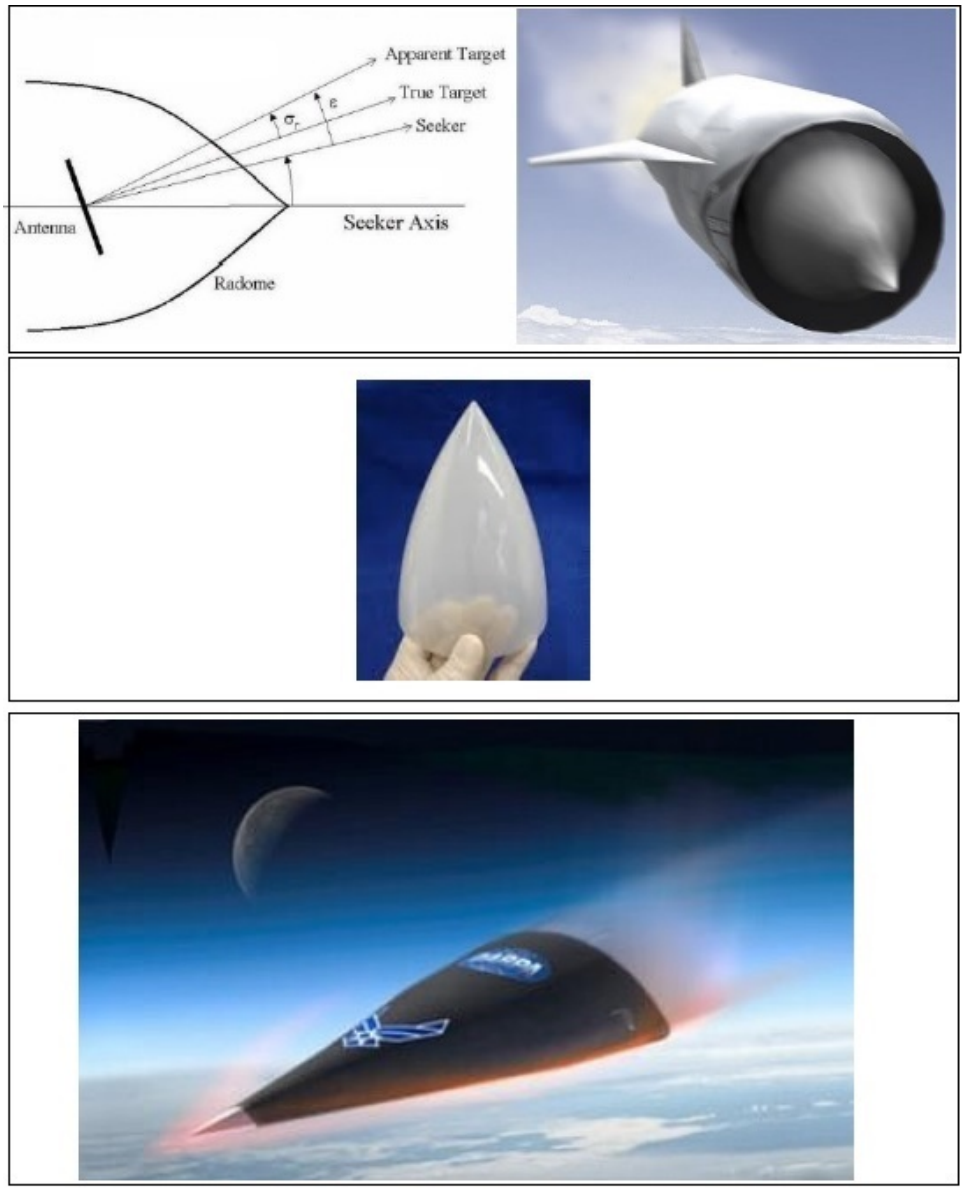

Figure 1.1. Radar dome illustration (top) used with permission [1]; Conic radome used with permission (middle); DARPA hypersonic vehicle rendering (bottom) used with permission [2].

1.2 Objective

Dielectric properties have been measured thoroughly for various applications, but not much is known for temperatures greater than $1,500^{\circ}$ Celsius [16]. Various methods to measure dielectric properties, such as lumped circuit, parallel plate capacitor, transmission line, cavity resonator, open resonator with hemispherical or spherical mirrors, and free-space methods [17]. This thesis utilized the cavity resonator method to design a novel approach for measuring dielectric properties at high temperatures due to the highly accurate sensitivity of the structure.

COMSOL Multiphysics is the software used to model the multi-physics required for this research by simulating a cylindrical cavity resonator and waveguide. The TE_{10} mode is dominant for such waveguides, which will be applied to the system [9]. The design of this model is the crux of this thesis. Modeling in COMSOL Multiphysics will assist in the investigation of the analytical and numerical approaches to find the optimal structure for the enhancement of the composite material properties, such as transmittance, thermal transfer, and others. The overall thesis outcome is to scale down the current method of obtaining material characteristics with furnace heating by designing a cavity resonator configuration that can be used experimentally to improve material quality and performance, a methodology which has never been attempted.

The electromagnetic spectrum describes all known frequencies and their respective wavelengths. The infrared frequencies range from 300 Terahertz (THz) to 300 Gigahertz (GHz), whereas microwaves range from 300 GHz to 300 Megahertz (MHz), highlighted in red in Figure 1.2 [9]. The focus of this research is to design the cylindrical cavity resonator at 10 GHz. However, with the interest of dual-spectrum common apertures for radomes and windows paired with mid-wave infrared of 4 to 6 μm increasing, this research could prove to be invaluable across the range of 300 THz to 300 MHz altogether, specifically in the X-band of 8-12 GHz centered at 10 GHz [18].

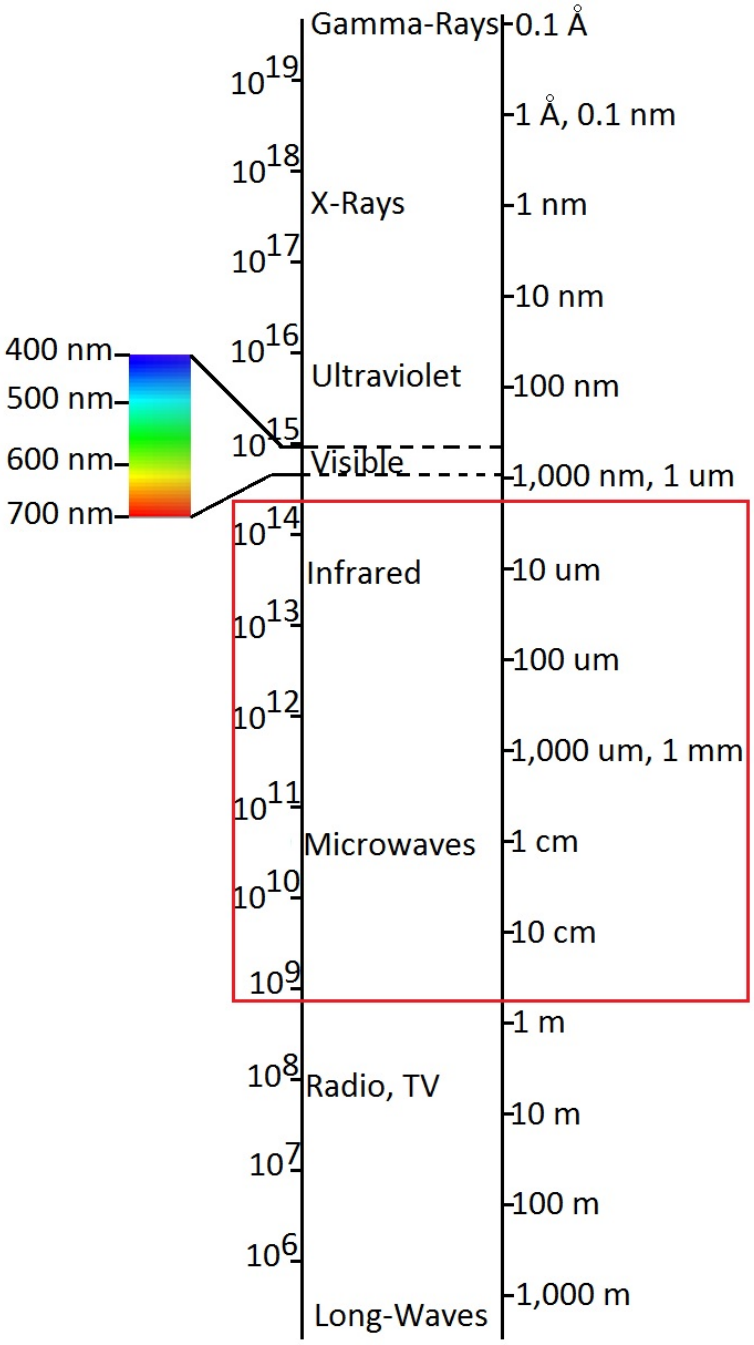

Figure 1.2. Electromagnetic spectrum with research focus highlighted in red; recreated from [3].

The specific research objectives are:

1. Design and model cylindrical cavity using analytic approximation at 10 GHz
2. Determine the feasibility of the technique to capture permittivity sensitivity
3. Simulate cavity perturbation of rod and disk samples to validate design
4. Generate new approximations to calculate the dielectric constant from empirical data
5. Establish an optimum cavity structure

1.3 Thesis Overview

- Chapter I: States the motivation and establishes objectives
- Chapter II: Discusses the background and theory presented in relative literature
- Chapter III: Describes the modeling used for this research
- Chapter IV: Presents the results and analysis of this research
- Chapter V: Summarizes conclusions and recommends future research

II. Background & Theory

2.1 Chapter Overview

Chapter II will cover the background necessary to bring the reader up to speed in order to understand the theory behind the research. The background focuses on the hypersonic environment, the radome or window structure, dual-spectrum, common aperture, microwaves, resonance, and permittivity. These are followed by the theory of how COMSOL Multiphysics® is used, dielectric measurement techniques, as well as a discussion of the previous research that was conducted that led to this thesis' research.

2.2 Background

2.2.1 Hypersonic Simulation

Hypersonic vehicles can easily reach temperatures higher than $1,500^{\circ}$ Celsius by aerodynamic heating. To simulate these extreme temperatures achieved in hypersonic travel, the materials tested within the cylindrical cavity resonator will be laser heated by a source such as a CO_2 laser. The focus of the laser beam will travel incident to a disk-shaped sample of the material, easily climbing to temperatures exceeding $1,500^{\circ}$ Celsius, a range of particular interest attained by such hypersonic vehicles. In contrast, laboratory-sized ovens or furnaces are currently used to heat large-sized materials [16], which utilize the free-space method to measure the dielectric properties of these materials. This process proves to be costly and time-consuming when screening hundreds of materials for scientific research, as the materials required for this method are expensive and difficult to manufacture. It is more practical to utilize small samples, which allow researchers to screen more types of materials at a faster

rate and significantly reduces costs and man-hours before using large samples for final experiments.

2.2.2 Radomes

To advance the utilization of hypersonic vehicles, new approaches must be sought out to thermally protect sensors from extreme environments [19]. Radomes and windows in light of this research are structural, impermeable enclosures that will be used to protect radar and sensor systems alike. They must be designed with the appropriate material to minimally attenuate electromagnetic signals to be transmitted and received by the radar or sensor [12]. These radomes and windows can be constructed in various shapes, dependent on the application. For example, hypersonic vehicles and missiles ubiquitously require conic radomes, as previously shown, so that they may best remain resilient in extreme environments.

Although most window or radome materials face inherent stress in an extreme temperature environment, added complications can stem from erosion or fractures when the hypersonic vehicle transits through rain or other debris. However, there has been substantial research that has shown different materials can exhibit better qualities than the once formidable single crystal sapphire windows that once represented state of the art properties for windows and radomes in extreme environments. Sapphire is typically the first candidate of choice when choosing high temperature suitable material [20], due to its strength. Fused silica is usually another choice as well, due to its reduced thermal stress in applications for high temperature environments. FR-4, or FR4, is a grade designation assigned to glass-reinforced epoxy laminate sheets, tubes, rods, and printed circuit boards. FR-4 is a composite material composed of woven fiberglass cloth with an epoxy resin binder that is flame resistant. "It is a popular and versatile high-pressure thermo set plastic laminate grade with good strength

to weight ratios. With near zero water absorption, FR-4 is most commonly used as an electric insulator possessing considerable mechanical strength [21]." However, the polymer is incompatible with high temperatures and lacks dual-spectrum band transmission properties. Novel nanocomposite ceramic materials such as aluminum oxynitride (ALON) and spinel have come to the forefront of such research [11]. Other advances have come with processing and manufacturing high quality and uniform materials for both spectral windows, allowing for optical transparency. These materials offer flexibility with respect to the composition and processing in a way that bulk single crystals are lacking, which may be explored to address the thermo-electro-mechanical issues in the hypersonic environment. The interest in high temperature electrical behavior arose from applications where high speed aerodynamic heating, reentry heating, radiant heating, or high power dissipation cause the surface or ambient temperature of the dielectric material to reach very high values [12]. This research is imperative for such applications as the SR-72, shown as Figure 2.1.

Figure 2.1. SR-72, hypersonic aircraft example used with permission [4].

Window and radome structures must be low-loss materials, have a low dielectric constant, and have a loss tangent that is less than 0.01 [16]. These properties must be taken into consideration during design in order to reduce any negative impact on the antenna performance within the radome. For most applications, homogeneous, single-layered radomes suffice due to the simple fabrication process, as well as low costs. Some examples of such materials include glass-fiber reinforced plastics

(GFRP), ceramics, elastomers, and monolithic foam [22]. Although the optimum thickness for single-layered radomes is approximately a half-wavelength, most single-layered radomes are usually thin with less than 0.02λ thickness in order to reduce the weight [23]. It is this thickness that makes these radome materials inadequate for survival in extreme environments. To circumvent this shortcoming, multi-layer or sandwich designs were developed, shown in contrast to the monolithic design in Figure 2.2. A common radome wall structure uses three layers consisting of two relatively higher permittivity thin skins and a thicker low-density core, known as the A-sandwich. This configuration is shown to exhibit high strength-to-weight ratios so that resonant elements, such as bandpass or bandstop filters, can be embedded within the core layer as well [23]. While these multi-layered wall compositions allow for RF capabilities, there arises the issue of temperature gradient effects in the hypersonic environment due to the mismatch of thermal expansion coefficients between the layers. To combat this issue, silicon nitride has shown to exhibit promising characteristics due to its graded porous properties. This porosity and dielectric constant relation is shown to be analytically coupled to thermo-mechanical characteristics in the electromagnetic frequency range from 1 GHz to 100 GHz [16]. Still, this advancement requires validation with measurements under the desired temperature in more depth.

In the infrared realm, a variety of materials with a monolithic structure have been developed for both active and passive optical windows, which include ALON, spinel, YAG, and sapphire [24]. These materials are known to be viable candidates for durability against sand or rain and the ability to operate in extreme temperature environments. Although these materials have shown transmittance above 80% in the mid-wave infrared range, more research is needed to find materials in the long-wave infrared range. Additionally, research was conducted on thermal flow and stress ef-

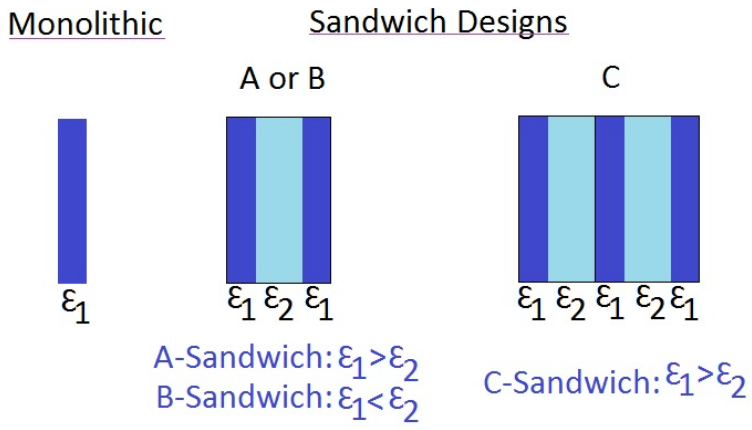

Figure 2.2. Different layered compositions for radomes structures–recreated from [5].

fects on the infrared sensor's performance, window position, and additional structures, such as active cooling systems in the supersonic environment and not the hypersonic environment, which requires additional study [25]. This is so that temperatures above 1,500° Celsius can be observed when traveling above Mach 5. In either case, there has been significant breakthroughs in achieving fully dense materials, eliminating optical scattering centers, and developing high purity precursor materials to improve transparency. Material development techniques for optimizing common aperture windows sustainable in extreme environments have yet to be fully investigated, which differentiates he design of this thesis to the current technique [11].

2.2.2.1 Dual-Spectrum Motivation

Optical and electromagnetic structures for infrared and microwave windows or radomes play a critical role in sensor configurations on various flying platforms [23]. In particular, hypersonic vehicle sensors are protected by these structures in extreme temperatures at speeds greater than Mach 5 [16]. In general hypersonic flight conditions, shockwaves can be generated by aerodynamic heating and high surface pressure [26]. Together, this heat, shock, and pressure can completely degrade the sensor's protective structure by altering its physical shape or mechanical properties. This shock-

wave propagation could distort images when captured by electro-optical/infrared sensors by shaking the protective structure or sensor itself. These high temperatures and non-uniform heating could also reduce the transmittance of the protective structure, which could degrade the sensitivity of the infrared or microwave sensors. Even self-emission of the high temperature sensor window or radomes has an effect on infrared images when added to the scene's radiation, altering the true radiation input and effectively blinding the sensor. To better understand these issues, this research looks to advance sensor protective structures by developing a better understanding of the relevant physics and utilizing cavity perturbation in order to do so. This will be critical to designing next generation sensor systems for hypersonic vehicles. The demand for multi-spectral sensors has also grown in response to improving communications, target detection, and tracking missions. These missions range across the electromagnetic spectrum and are shown in Figure 2.3, which provides a physical size to scale.

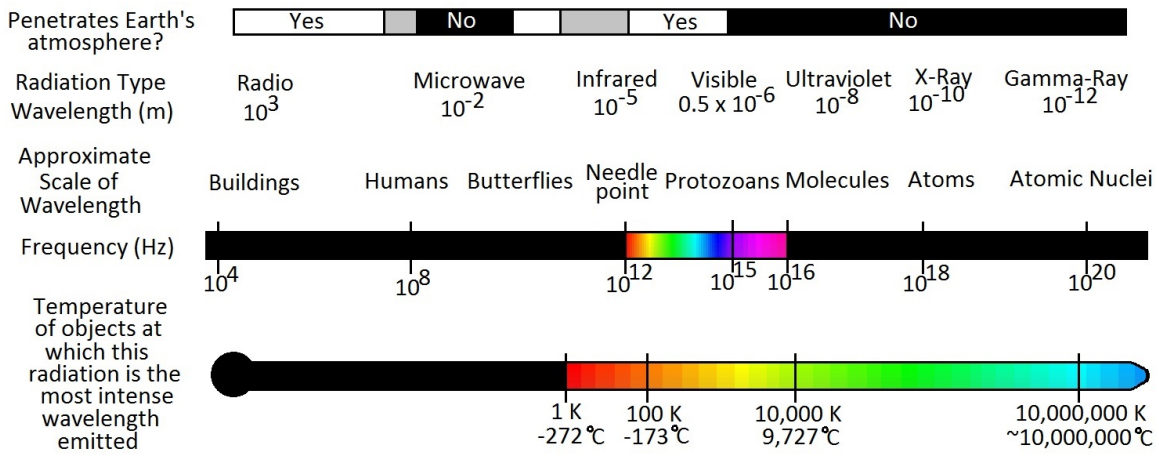

Figure 2.3. Recreated illustration of electromagnetic spectrum [6].

2.2.2.2 Common Aperture

A common aperture is an electromagnetic/optical window structure that can be used to protect multi-mode sensors from its environment. These structures must

not only physically protect the sensor, but they must also be able to support and enable the sensor's operation. Dielectric, thermal, and mechanical properties must be taken into account when designing a common aperture. These requirements will aid in ensuring transparency for the multi-mode sensors and acceptable structural performance. The research in this field can be applied to radiation pattern shaping, coupling, and sub-wavelength imaging, which could lead to the modeling of radio frequency and electro-optical/infrared applications.

2.2.2.3 Cavity Perturbation Technique

In order to obtain suitable candidate materials for radomes or windows, dielectric properties have often been measured using the cavity perturbation technique. As an electromagnetic signal is sent through a waveguide into a cylindrical cavity, the resonant frequency is measured from the scattering parameters (S-parameters) of the signal, which are measured using a network analyzer [27]. However, when introducing a sample into the cavity, the material perturbs the electric field and shifts the resonant frequency of the cavity [28]. This research intends to use changes in the properties of a sample to perturb the cavity as its focus. With both the resonant frequencies of the empty cavity and the perturbed cavity, these values can also be used to calculate the Quality (Q) factors of the cavity, which in turn aids in finding the imaginary part of the complex permittivity, also called the dielectric loss tangent. Knowing the real and imaginary parts leads to the complex permittivity of the cavity itself [29]. These properties can lead to the research of appropriate materials to create a common aperture to be used as radomes and windows sustainable in extreme temperatures. The equations to find the complex permittivity, Q-factor, and loss tangent will be discussed in the following chapters.

2.2.3 Microwaves

Microwave is a term used to identify any electromagnetic waves above 1 GHz up to, and including, 300 GHz because of the relatively short physical wavelengths at these frequencies [9]. Short wavelength energy offers distinct advantages in many applications. For instance, sufficient directivity can be obtained using relatively small antennas and low-power transmitters. These characteristics make microwave frequencies ideal for both military and civilian uses of radar and communication applications. Small antennas and other small components, such as cellular phones, are made possible by microwave frequency applications. This size advantage can be considered when designing solutions limited with space, weight, or both. However, microwave frequencies can present their own issues with transmission, generation, and circuit design that are not encountered at lower frequencies. While conventional circuit theory is based on voltages and currents, microwave theory is based on electromagnetic fields. Techniques can be described qualitatively as microwave when the wavelengths of signals are roughly the same as the dimensions of the apparatus, so lumped-element circuit theory is inaccurate for the microwave applications. Thus, practical microwave techniques tend to move away from discrete resistors, capacitors, and inductors used with lower frequency radio waves. Instead, distributed circuit elements and transmission-line theory are more useful methods for microwave engineering. Open-wire and coaxial transmission lines give way to waveguides and stripline, and lumped-element tuned circuits are replaced by cavity resonators or resonant lines. Effects of reflection, polarization, scattering, diffraction, and atmospheric absorption associated with visible light are of practical significance in the study of microwave propagation. The same equations of electromagnetic theory apply at all frequencies. Microwave properties of materials are determined by resonant cavity techniques that measure the shifts of resonant frequencies due to the sensitivity and accuracy of the structure itself [30].

2.2.3.1 Resonance

In physics, resonance describes when a vibrating system or external force drives another system to oscillate with greater amplitude at a specific preferential frequency. Amplitude increases as damping decreases and frequency approaches resonant frequency of a driven damped simple harmonic oscillator. Frequencies at which the response amplitude is a relative maximum are known as the systems' resonance or resonant frequencies. At resonant frequencies, small periodic driving forces have the ability to produce large amplitude oscillations. This is because the system stores vibrational energy. Resonance occurs when a system is able to store and easily transfer energy between two or more different storage modes, such as kinetic and potential energies in the case of a pendulum, for example. However, there are some losses from cycle to cycle, called damping. When damping is small, the resonant frequency is approximately equal to the natural frequency of the system, which is a frequency of unforced vibrations. Some systems have multiple and distinct resonant frequencies. Resonance phenomena occurs with all types of vibrations or waves, such as mechanical, acoustic, electromagnetic, nuclear magnetic, electron spin, and quantum wave function resonances. Resonant systems can be used to generate vibrations at a specific frequency, such as musical instruments, or pick out specific frequencies from a complex vibration containing many frequencies, such as filters.

2.2.4 Permittivity

As microwaves propagate towards material, the energy is either reflected or transmitted at the surface, where part of the latter can also be absorbed [31]. These three outcomes constitute the definition of dielectric properties. Fundamentally, the electrical property by which these interactions are described is called the complex relative

permittivity of a material, ϵ^*, or

$$\epsilon^* = \epsilon' + j\epsilon'', \tag{2.1}$$

where ϵ' is called the dielectric constant and ϵ'' is called the dielectric loss factor [32]. Permittivity affects the propagation of electric fields. To demonstrate how this is accomplished, the top of Figure 2.4 depicts two charged and separate plates with equal and opposite charges, while assuming there is no material between the plates (i.e. vacuum). An electric field exists in the top of Figure 2.4, which points downward from the positive charge to the negative charge. On the other hand, the bottom of Figure 2.4 depicts the same plates with a material between them. This material can be composed of molecules that resemble an electric dipole, which are two point electric charges of opposite polarity located close together.

In this case, a water molecule is represented by the top of Figure 2.5. Generally speaking, materials, such as water, are composed of molecules or atoms, which often have the form of a dipole moment as previously described. In the absence of such an external electric field as shown in the top of Figure 2.4, the molecules are randomly aligned. This sporadic alignment can be seen in the bottom of Figure 2.5.

Referring back to the bottom of Figure 2.4, where the material is placed between the plates, the water molecules realign themselves along their dipole moment and the external electric field. As shown in the bottom of Figure 2.4, the electric field due to the dipole moments of such water molecules inherently oppose the external electric field, thereby reducing the net electric field within the material. Permittivity, often varied with frequency and temperature, is a measure of how much the molecules oppose the external electric field. The equation for an electric field due to a single

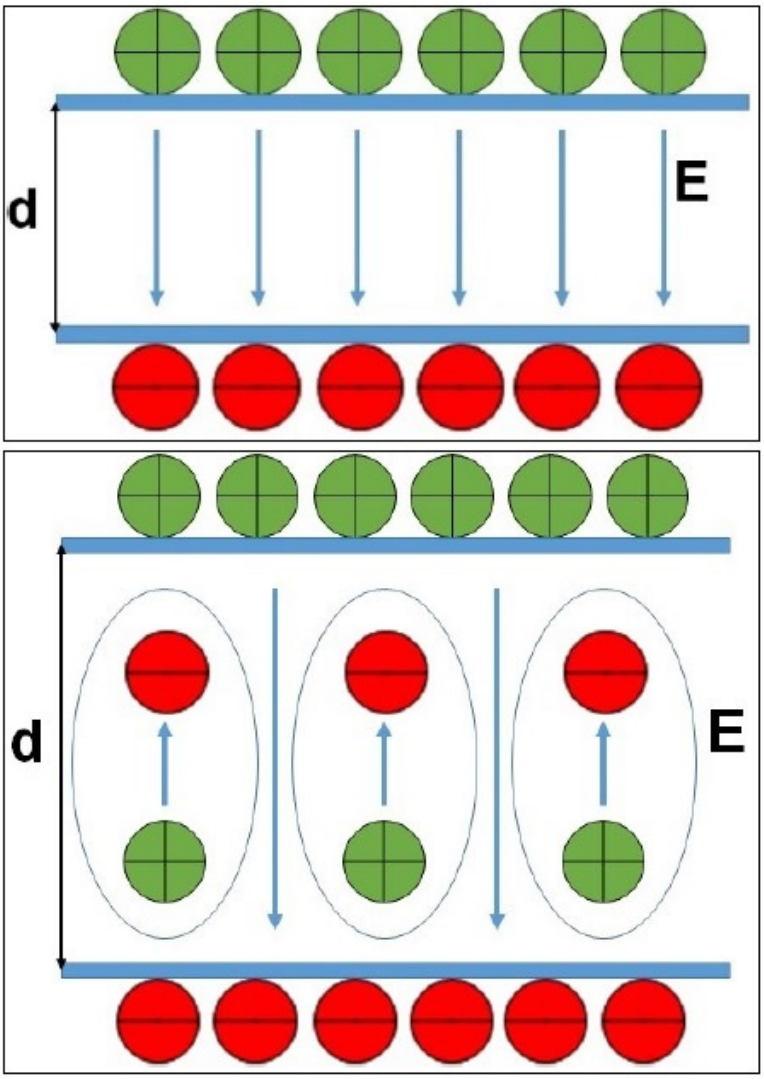

Figure 2.4. Empty electric field created by two oppositely charged plates (top); Electric field with material between two oppositely charged plates (bottom)–recreated from [7].

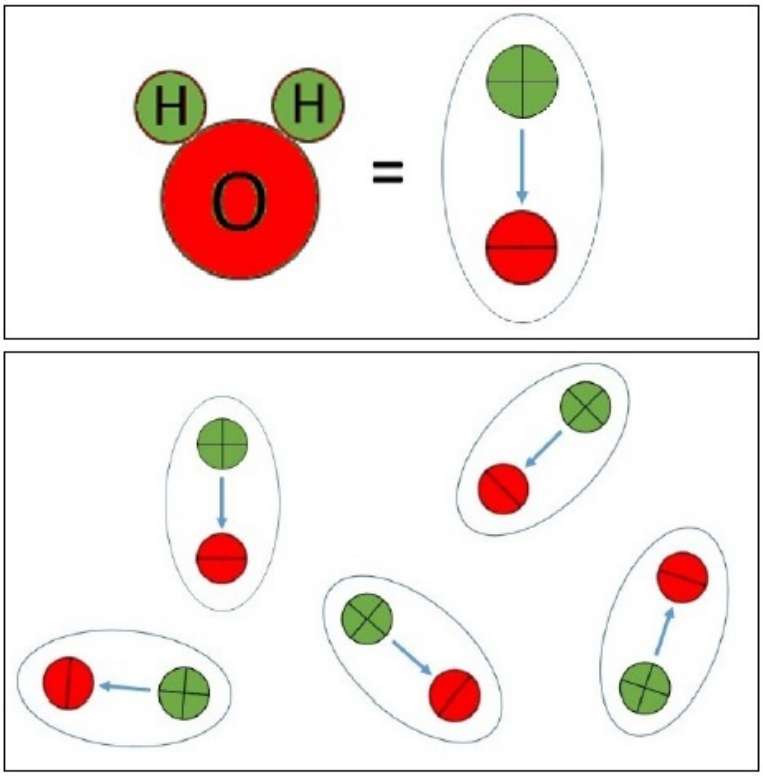

Figure 2.5. Water molecule is depicted by an electric dipole moment–recreated from [8].

point charge, q in Coulombs, at a distance, R, is given by

$$|\mathbf{E}| = \frac{q}{4\pi\epsilon_0 R^2}\,[V/m], \tag{2.2}$$

where the permittivity of free space, ϵ_0, equals 8.854×10^{-12} [Farads/meter]. The permittivity of free space is the permittivity of a vacuum, where no atoms are present. By adding a material into this vacuum, the electric field due to a point charge will be reduced due to the molecules within a material, which modifies Equation 2.2 to become

$$|\mathbf{E}| = \frac{q}{4\pi\epsilon_r\epsilon_0 R^2}\,[V/m], \tag{2.3}$$

where ϵ_r is called the relative permittivity [33]. In this research, the focus will not be with the complex permittivity itself as in Equation 2.1, but will concentrate on the real part of the complex permittivity, or simply

$$\epsilon' = \epsilon_r\epsilon_0. \tag{2.4}$$

As ϵ' is always greater than or equal to 1.0, the electric field in Equation 2.3 will always be reduced relative to the electric field in free space. This reduction is the measure of permittivity. Materials that have low conductivity and a dielectric constant greater than 1.0 are known as dielectrics. With respect to Maxwell's Equations, permittivity creates the constitutive relationship between the electric flux density and the electric field, or

$$D = \epsilon' E\,[C/m^2] \tag{2.5}$$

Additionally, the speed of light in free space is related to the permittivity and per-

meability of the medium, where

$$c_0 = \frac{1}{\sqrt{\mu_0 \epsilon_0}} = 2.998 \times 10^8 [m/s] \tag{2.6}$$

and the speed of light in a dielectric is

$$c = \frac{1}{\sqrt{\mu_0 \epsilon_r \epsilon_0}} [m/s] \tag{2.7}$$

From Equations 2.6 and 2.7, it is shown that the speed of light is reduced in a dielectric relative to the speed in a vacuum. Moreover, the wavelength for an electromagnetic wave of a given frequency, f, is smaller in a dielectric than it is in a vacuum, where

$$\lambda_0 = \frac{c_0}{f} [meters] \tag{2.8}$$

for free space and

$$\lambda = \frac{c}{f\sqrt{\epsilon_r}} [m] \tag{2.9}$$

for a dielectric material.

In electromagnetism, permittivity is the measure of resistance that is encountered when forming an electric field within a medium. In other words, permittivity is a measure of how an electric field affects and is affected by a dielectric medium. The permittivity of a medium describes how much electric field (electric flux) is generated per unit charge in the medium. More electric flux exists in a medium with a low permittivity (per unit charge) because of polarization effects. Permittivity is directly related to electric susceptibility, which is the measure of how easily a dielectric polarizes in response to an electric field. Thus, permittivity relates a material's ability to resist an electric field. Conversely, permeability is the measure of the ability of a material to support the formation of a magnetic field within itself. Hence, it is the

degree of magnetization that a material obtains in response to an applied magnetic field. Magnetic permeability is typically represented by μ. Coined by Oliver Heaviside in 1885, permeability is measured in Henries per meter (or Newtons per ampere squared), whose reciprocal is magnetic reluctivity. The permeability constant, μ_0, also called the magnetic constant or permeability of free space, is the measure of the amount of resistance encountered when forming a magnetic field in a vacuum. The permeability of free space is equal to $1.2566 \times 10^{-6}\,[H/m]$. As with electric susceptibility, magnetic susceptibility is a dimensionless proportionality factor that indicates the degree of magnetization of a material in response to an applied magnetic field. It is important to distinguish between permittivity and permeability as permittivity is the focus of this research and permeability will be assumed to equal one. Also, the permittivity-high-temperature correlation in previous research concluded that as temperature increases, permittivities increase [13, 14].

2.3 Theory

2.3.1 Computational Modeling Tool

COMSOL Multiphysics® is a commercial computational tool that is capable of designing and simulating the optimal structure for a common radio frequency and infrared window under the desired environment. This thesis focuses on the radio frequency spectrum. COMSOL Multiphysics® will be used to simulate the cavity perturbation technique due to its ability to couple physical interactions among several phenomena. COMSOL Multiphysics® is a general-purpose finite element software platform, based on advanced numerical methods, for modeling and simulating physics-based problems. With COMSOL Multiphysics®, one can account for coupled or multiphysics phenomena. One can further expand the simulation platform with dedicated physics interfaces and tools for electrical, mechanical, fluid flow, and

chemical applications. Additional interfacing products also connects COMSOL Multiphysics® simulations with technical computing, CAD, and ECAD software. This will aid in measuring and calculating the complex permittivity.

2.3.2 Cavity Perturbation Technique

A cavity resonator is a hollow closed conductor, such as a metal box or cavity within a metal block, which contains electromagnetic waves reflecting back and forth between the cavity walls. When applying a radio wave source at one of the cavity's resonant frequencies, the oppositely moving waves form standing waves and the cavity stores electromagnetic energy. Since the cavity's lowest resonant frequency, called the fundamental frequency, f_0, is that at which the width of the cavity is equal to a half-wavelength, $\lambda/2$, cavity resonators are only used at microwave frequencies and above, since the wavelengths are short enough so that the cavity is conveniently small in size as well [34]. To design a cavity that can be used with the cavity perturbation technique, a resonant frequency must first be selected. Again, this research narrows in on 10 GHz. The cylindrical cavity resonator is placed in a rectangular waveguide, which is designed to resonate at 10 GHz, and will utilize Equation 2.11 to calculate the required radius of the cylindrical cavity.

To understand how a cavity resonator operates, a rectangular waveguide cavity can be used to explain how resonators work. As waveguides are a type of transmission line, resonators can be constructed from closed sections of a waveguide [9]. Due to the radiation loss from an open-ended waveguide, waveguide resonators are usually short-circuited at both ends, thus forming a closed box or cavity. Electric and magnetic energy is stored within the cavity and power can be dissipated in the metallic walls of the cavity, as well as in the dielectric sample inside of the cavity. Coupling to the resonator can be by a small aperture, which is what is used in this thesis, or by a small

probe or loop. Such coupling devices are required to transfer energy from the input to the resonator. A Coupling probe can be formed by extending a feeding coaxial cable at a small distance into the cavity resonator, which creates an electric field between the probe and the adjacent wall of the cavity. This field then radiates energy into the resonator like a small antenna. On the other hand, a coupling loop can be formed by grounding (touching) that same probe directly to the cavity, where the center of the loop is located midway between the top and bottom cavity walls. In either case, the size of the probe or loop must be small in comparison to the wavelength [17]. Pozar derived the resonant frequencies for the general TE_{mnl} or TM_{mnl} resonant modes, which found the resonant frequency for a rectangular cavity to be given by

$$f_{mnl} = \frac{c}{2\pi\sqrt{\mu_r\epsilon_r}}\sqrt{(\frac{m\pi}{a})^2 + (\frac{n\pi}{b})^2 + (\frac{l\pi}{d})^2}[Hz], \tag{2.10}$$

where a, b, and d are the various lengths of the rectangular resonant cavity as shown in Fig 2.6 [9].

If $b < a < d$, then the dominant resonant mode, which is also the lowest resonant frequency, will be the TE_{101} mode, corresponding to the TE_{10} dominant waveguide mode in a shorted guide of length $\lambda/2$. The dominant TM mode is the TM_{110} mode [9]. This electromagnetic wave is then supplied to the cylindrical cavity. With the dominant circular waveguide modes defined by TE_{nml} and TM_{nml}, this translates the dominant rectangular waveguide input to TM_{01} for a cylindrical cavity's dominant mode, where the resonant frequency is given by

$$f_{nml} = \frac{c}{2\pi\sqrt{\mu_r\epsilon_r}}\sqrt{(\frac{p_{nm}}{a})^2 + (\frac{l\pi}{h})^2}[Hz], \tag{2.11}$$

where p_{nm} is the propagation constant and equal to 2.405 [9]. TM_{01} is often used to characterize radio frequency materials due to its sensitivity [13, 35]. Fig 2.7 depicts

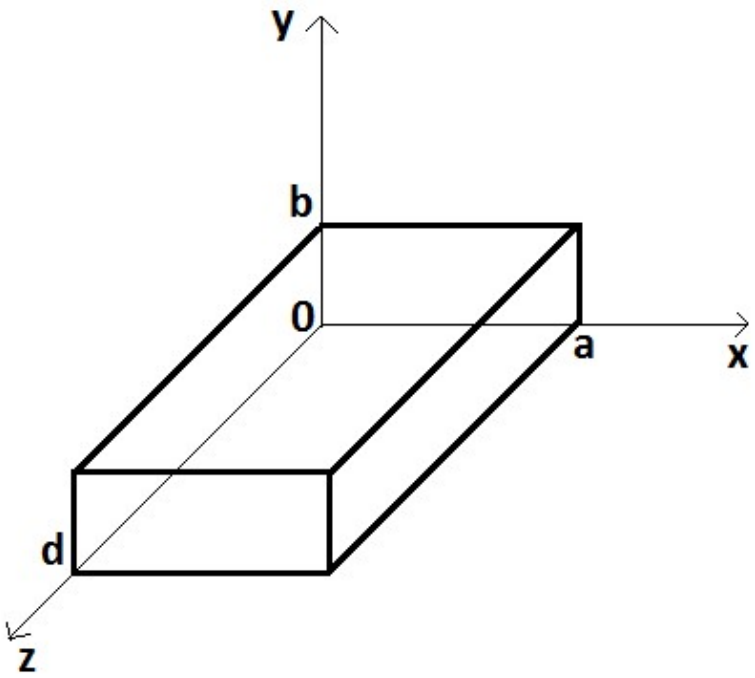

Figure 2.6. Rectangular cavity illustration recreation [9].

such a cylindrical cavity, where a is the radius and d is the height.

The design of this thesis is to couple a rectangular waveguide to a cylindrical cavity resonator. In order to do so, the resonator will be excited by aperture coupling [9].

The focus of this research was utilizing the real part of the complex permittivity, as this is the component measured by the network analyzer. However, for rod-shaped samples in a cylindrical cavity, where the radius of the rod is much smaller than the radius of the cavity, in the TM_{010} mode, von Hippel derived equations for approximating the complex dielectric properties of a material were the real and imaginary terms [36],

$$\epsilon' = 1 + 0.539 \times \frac{V_c(f_0 - f_s)}{V_s f_0} \tag{2.12}$$

and

$$\epsilon'' = 0.269 \times \frac{V_c}{V_s} \times (\frac{1}{Q_s} - \frac{1}{Q_0}), \tag{2.13}$$

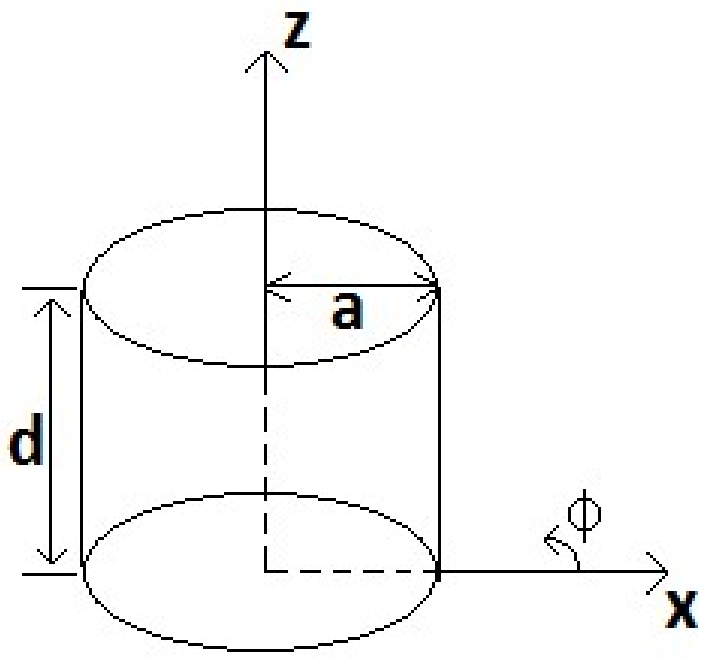

Figure 2.7. Cylindrical cavity illustration recreation [9].

respectively, where V_C is the volume of the cavity, V_S is the volume of the sample, f_0 is the resonant frequency of the empty cavity, f_S is the resonant frequency of the cavity with the sample, Q_S is the Q-factor of the cavity with the sample, and Q_0 is the Q-factor of the empty cavity [17]. ϵ' represents the stored energy within the cavity and ϵ'' relates to the dissipation, or loss, of energy in the cavity. The Q-factors can be calculated by

$$Q_0 = \frac{f_0}{\triangle f_{0_{3dB}}} \tag{2.14}$$

and

$$Q_S = \frac{f_S}{\triangle f_{S_{3dB}}}, \tag{2.15}$$

where $\triangle f_0$ and $\triangle f_S$ are the resonance widths or full width at half maximum at 3dB for the empty and perturbed cavities, respectively [12].

The measurements of dielectric properties have been studied extensively through various methods. The focus of this research is to utilize the cavity perturbation

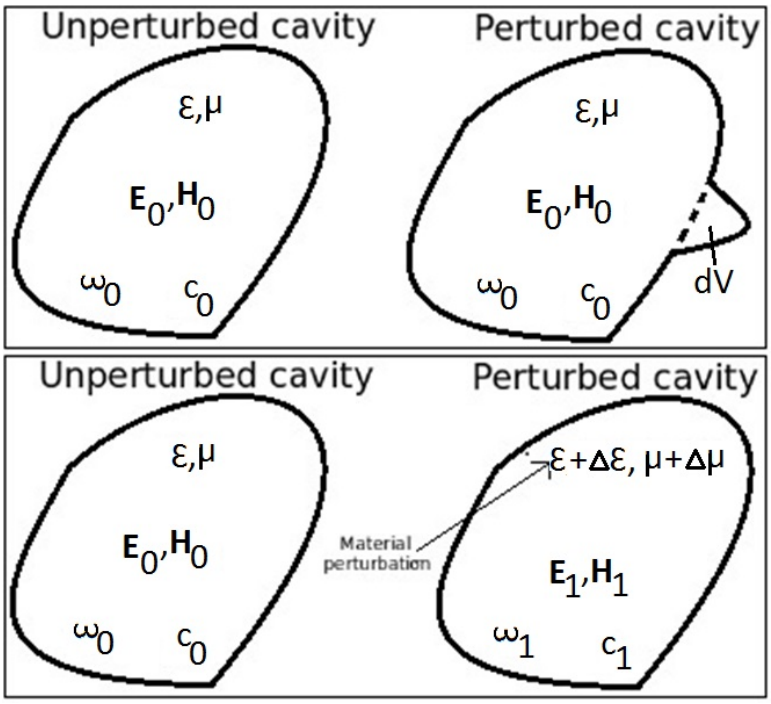

Figure 2.8. Cavity perturbation technique with small boundary deformation (top); Cavity perturbation technique with a foreign material primer (bottom); recreated from [9].

method. According to Pozar [9], there are two variations of the cavity perturbation technique. The first is achieved by a small boundary deformation of the cavity, shown at the top of Figure 2.8. This can be demonstrated by inserting and removing a screw, composed of the same material as the cavity, thus changing the volume of the cavity. The second variation, and most commonly used due to its simplicity, is obtained by introducing a foreign material into the cavity, shown as the bottom of Figure 2.8, which offers a high degree of accuracy [37]. This thesis utilizes the second variation of the cavity perturbation method. If $\boldsymbol{E}_0$ and $\boldsymbol{H}_0$ are the fields of the original cavity, and $\boldsymbol{E}_1$ and $\boldsymbol{H}_1$ are the fields of the material filling the cavity, then Maxwell's curl equations can be written for the two cases as:

$$\bigtriangledown \times \boldsymbol{E}_0 = -j\omega_0\mu\boldsymbol{H}_0, \tag{2.16}$$

$$\bigtriangledown \times \boldsymbol{H}_0 = j\omega_0\epsilon\boldsymbol{E}_0, \tag{2.17}$$

$$\bigtriangledown \times \boldsymbol{E}_1 = -j\omega_1(\mu + \triangle\mu)\boldsymbol{H}_1, \tag{2.18}$$

$$and \bigtriangledown \times \boldsymbol{H}_1 = j\omega_1(\epsilon + \triangle\epsilon)\boldsymbol{E}_1, \tag{2.19}$$

where ω_0 is the resonant frequency of the empty cavity and ω_1 is the resonant frequency of the perturbed cavity. Assuming $\triangle\epsilon$ and $\triangle\mu$ are small, the perturbed fields, $\boldsymbol{E}_1$ and $\boldsymbol{H}_1$, can be approximated by the original fields, $\boldsymbol{E}_0$ and $\boldsymbol{H}_0$, and ω_1 by ω_0 to give the fractional change in resonant frequency as

$$\frac{\omega_1 - \omega_0}{\omega_0} \approx \frac{-\int \triangle\epsilon|\boldsymbol{E}_0|^2 + \triangle\mu|\boldsymbol{H}_0|^2 dv}{-\int \epsilon|\boldsymbol{E}_0|^2 + \mu|\boldsymbol{H}_0|^2 dv}, \tag{2.20}$$

noting the numerator and denominator are integrated over the volume, which shows that any increase in ϵ or μ at any point in the cavity results in a decrease in the resonant frequency. Equation 2.20 is valid to a high degree of accuracy, but will only be realized if the sample shape and position within the cavity are considered [38]. The terms in Equation 2.20 can be related to the stored and magnetic energies in the original and perturbed cavities as well, so that the decrease in resonant frequency can be related to the increase in stored energy of the perturbed cavity [17]." What separates the research of this thesis from others is the goal of correlating said cavity perturbation method with temperature dependence, whose eventual state is to develop a function of complex permittivity with respect to temperature, or $\epsilon(T)$. Various papers have also conducted cavity perturbation in the microwave frequency range of particular interest to this thesis [37, 39, 34, 40, 41].

2.3.3 Dielectric Measurement Techniques

While this research focuses on utilizing the cavity perturbation technique, other dielectric property measurement techniques exist. The lumped circuit technique is no longer used since it was designed for low frequency and high loss applications. For parallel plate capacitors, the complex dielectric permittivity is obtained by measuring the change of capacitance and of conductance due to the device with and without a foreign material [42, 43]. The transmission line technique has been used to measure dielectric, granular, and liquid materials via the transmission-reflection and short-circuit line methods [44]. Although inexpensive and simple to perform, the transmission line technique can be quite cumbersome since the samples are quite large with slab or annular geometries. The mirror method uses an open-resonator construct to measure dielectric properties and can be of one of two types, hemispherical and spherical [45, 46, 47]. These methods operate in the 30-200GHz region, but can also be used in lower frequencies with large enough sample sizes.

Similarly, the free-space method also utilized large sample sizes, but makes it particularly suitable for materials at high temperatures and for inhomogeneous dielectrics [48, 49]. It is this method that is currently being used to measure dielectric materials at high temperatures within laboratory-sized oven or furnaces. Using the free-space method, a sample is placed between a transmitting antenna and a receiving antenna, as shown in Figure 2.9, and the attenuation and phase shift of the signal are measured [29]. The results of which can be used to infer the material dielectric properties.

Accurate measurement of the permittivity over a wide range of frequencies can be achieved by free-space techniques. In most systems, the accuracy of ϵ' and ϵ'' determined depends mainly on the performance of the measuring system and the validity of the equations used for the calculation. Multiple reflections, mismatches,

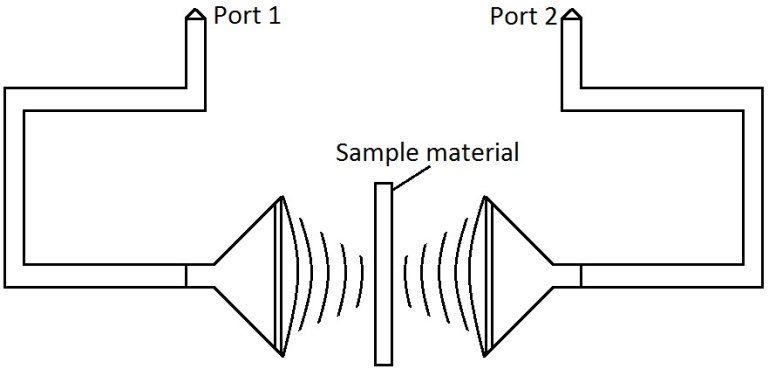

Figure 2.9. Free-space method; recreated from [10].

and diffraction effects at the edges of the sample are generally considered the main sources of errors. To enhance the measurement accuracy, special attention must be paid to the choice of the radiating elements, the design of the sample holder, and the sample geometry and location between the two radiating elements [29]. The resonator technique can also be used to measure dielectric properties, which is what the cavity perturbation technique stems from, and consists of a microwave resonator that is partly or completely filled with the material in question.

2.3.3.1 S-Parameters

S-parameters are elements of a scattering matrix and describe the electrical behavior of linear, electric networks that undergo various steady state stimuli from electromagnetic signals. These S-parameters are useful for electrical engineering, electronics engineering, communications design, and, most importantly for this research, microwave engineering [9]. To characterize a linear electric network, S-parameters use matched impedance loads. These terminations are much easier to use at higher signal frequencies than open-circuit or short-circuit terminations and the quantities are measured in terms of power, or Watts (W). Many electrical properties of networks of components, such as inductors, capacitors, and resistors, can be expressed in terms of S-parameters as gain, return loss, voltage standing wave ratio, reflection coefficient,

and amplifier stability. The term scattering is more common to optical engineering than radio frequency engineering, referring to the effect observed when an electromagnetic plane wave is incident on an interface or passes across dissimilar dielectric media. However, in the context of S-parameters, scattering refers to the way in which the traveling currents and voltages along a transmission line are affected when they meet a discontinuity caused by the insertion of a network into the transmission line. This is the equivalent to a wave meeting an impedance differing from the line's characteristic impedance. Although, applicable at any frequency, S-parameters are mostly utilized for networks operating in the radio frequency or microwave frequencies, where signal power and energy considerations are more easily quantified than voltages and currents. S-parameters change with the measured frequency, so frequency must be specified for any S-parameter measurements stated, as well as the characteristic or system impedances. Again, S-parameters are represented in matrix form and obey the rules of matrix algebra. To measure these S-parameters, network analyzer are often utilized to measure the network parameters of electrical networks. Network analyzers are often used to characterize two-port networks, such as amplifiers and filters, but they can be used on networks with an even larger, arbitrary number of ports. For this thesis, the network analyzer will be simulated by COMSOL Multiphysics® and measured S_{11}, the reflection of the input signal, and S_{21}, the transmission via Ports 1 and 2.

2.3.3.2 Q-factor

Q-factors are dimensionless parameters that describe how underdamped an oscillator or resonator is and characterizes a resonator's bandwidth relative to its center frequency [9]. Higher Q-factors indicate a lower rate of energy loss relative to the stored energy of the resonator, resulting in oscillations that dampen out more slowly.

For example, a pendulum suspended from a high-quality bearing, oscillating in air, has a high Q-factor, whereas a pendulum immersed in water has a low Q-factor. Due to the low resistance of their conductive walls, cavity resonators have qualitative Q-factors. In other words, their bandwidth, which is the range of frequencies around the resonant frequency by which they resonate, is very narrow. Thus they can used as narrow bandpass filters. Resonators with high Q-factors have low damping properties and ring longer. Due to time constraints, Q-factors will not be discussed in this research, but it is an important part to describing cavity properties when researching the complex permittivity of dielectric materials.

2.4 Previous Research

Previous to this research, Dr. James Park, the primary investigator from the Sensors Directorate, Air Force Research Laboratory, or AFRL/RYMH, had found promising results in modeling a rectangular waveguide with a rectangular cavity, shown in the top of Figure 2.10. As shown in Figure 2.10, the cavity was approximately 6cm long with a height of 1.016cm and a width of 2.286cm. The length of the rectangular cavity itself was 1.985cm. This empty rectangular cavity's resonant frequency, shown in the bottom of Figure 2.10, was 10.23 GHz as designed using Equation 2.10.

The next step was to find an optimal sample size for high temperature radio frequency material characterization, such as resonant frequency, heat distribution, thermal stabilization, and others. This was accomplished by parametrically sweeping various sample sizes (varied widths and heights), as shown in the top of Figure 2.11. The bottom of Figure 2.11 shows the associated resonant frequencies with the sample's varied widths and heights. Knowing these resonant frequencies, AFRL/RYMH was able to extract the permittivities of FR4 and silica glass at these varied sample

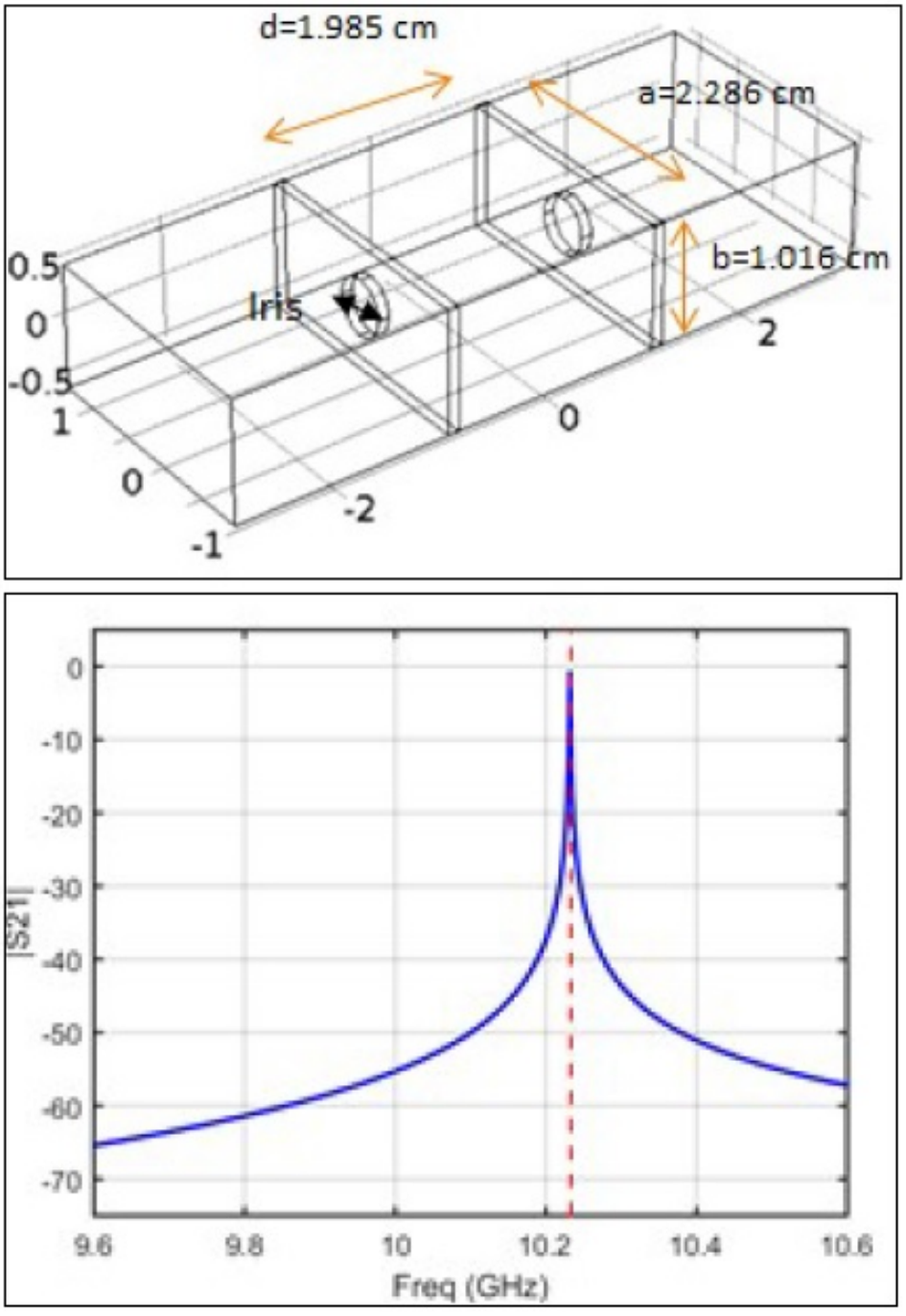

Figure 2.10. AFRL/RYMH's rectangular cavity design (top) used with permission; Empty rectangular cavity resonant frequency, 10.23 GHz (bottom) used with permission [11].

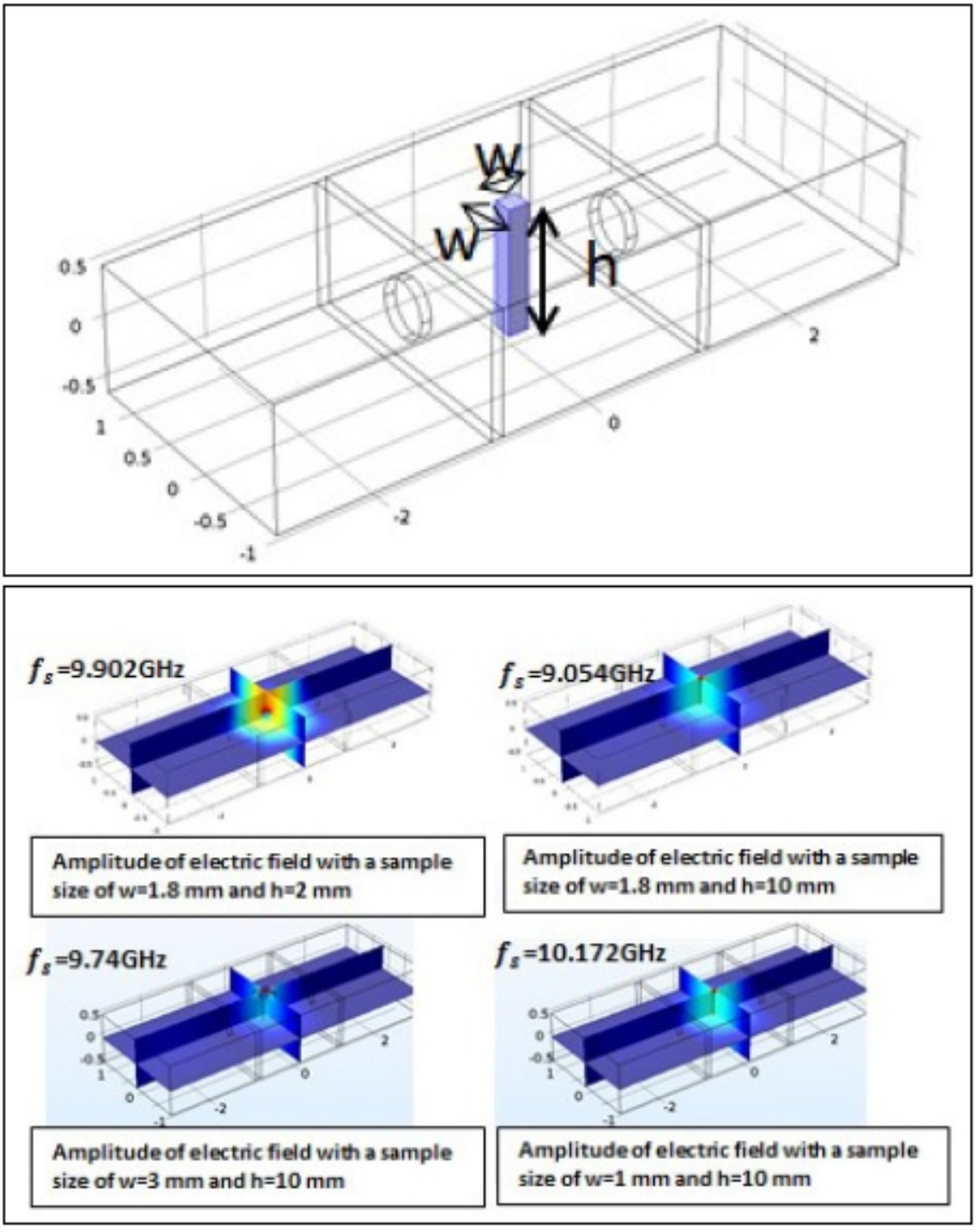

Figure 2.11. Rectangular cavity with sample material (top) used with permission; Rectangular cavity electric field amplitudes (bottom) used with permission [11].

dimensions, shown in Figure 2.12.

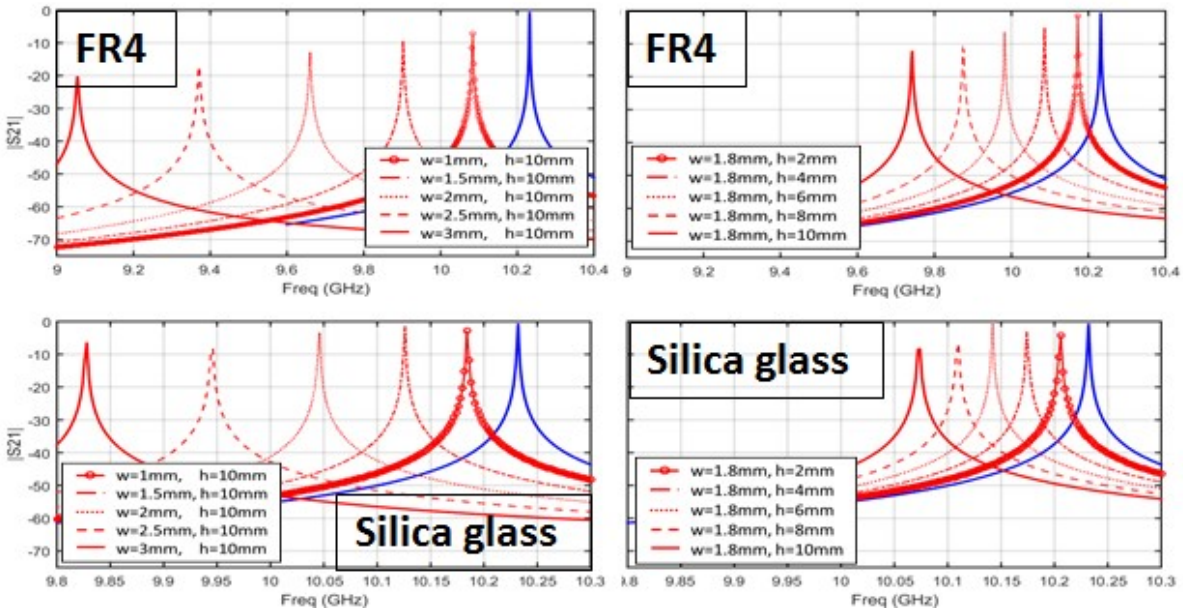

Figure 2.12. Rectangular cavity S-parameters for FR4 and silica glass used with permission [11].

This previous research showcases the computer-modeled rectangular waveguide and rectangular cavity's ability to measure dielectric properties as accurately as experimental setups. It also lays the foundation for the success of using a rectangular waveguide coupled with a cylindrical cavity, as demonstrated in this thesis.

2.5 Summary

With the background and theory having been discussed, the remainder of this thesis will discuss the design and modeling of a cylindrical cavity resonator used to simulate the cavity perturbation technique with rod and disk samples, the results calculated from the change in frequency, and the conclusions drawn from the results.

III. Design and Modeling

3.1 Chapter Overview

Real-world electromagnetic problems are not easily calculated analytically due to the physical geometries found in actual devices. With appropriate boundary conditions and constitutive relationships, computational numerical techniques can overcome the difficulty of deriving closed-form solutions of Maxwell's equations. This showcases why "computer modeling is the primary means of assessing the merit of a particular radome design during its development phase [50]." This enabler allows researchers to cope with new developments and applications, where the determination of an optimal microstructure for a desired application is important in the design process. The characterization of composite media has drawn considerable attention in various fields of science. However, it is also a daunting effort to modify the "constituent materials and internal microstructures to produce the required performance characteristics for multi-spectral applications [16]." Therefore, modeling can be tasked to address the optimization design issue in which an objective function including a set of physical properties (such as dielectric constants, thermal conductivities, and layer thicknesses) can be optimized with respect to the physical constraints on the wavelength, index of refraction, temperature, and mechanical durability. Through systematic iteration, the optimal design of a common aperture infrared window/radome can be realized by combining the proposed modeling technique of this research with the synthesis and prototype fabrication [16]. This chapter discusses COMSOL Multiphysics® and how it was used to design and simulate the cylindrical cavity along with the two different samples of a rod and disk.

3.2 COMSOL Multiphysics®

Attending a multitude of workshops aided in learning a small fraction of the power of modeling with the COMSOL Multiphysics® software. Starting with the wizard, the first step was to choose a 3-D Space Dimension, so that the finished model could be exported to CAD software to be built into a prototype. The next step was to add a physics interface, so the "Electromagnetics Physics Module" was chosen to begin designing the cavity. Then the "Frequency Domain Study" was selected to represent the solver that would be used for the computation. After choosing the study, the wizard then goes through the modeling process. As a rule of thumb, it was beneficial to create global parameters in order to easily assign variables throughout the modeling, while also enabling easier manipulation of the parametric sweeps later in the research [51]. The next step was to begin creating the geometries of the design. Finally, the studies were computed to find the resonant frequencies in order to calculate the permittivities. The following sections are a walkthrough for designing, modeling, and simulating the cavity of this thesis.

3.2.1 Physics Module

The electromagnetic signal used in the model was generated using the "Electromagnetic Waves, Frequency Domain Module." This radio frequency, electromagnetic waves, frequency domain interface is used to solve for time-harmonic electromagnetic field distributions [51]. For this specific physics interface, the maximum mesh element size should be limited to a fraction of the applicable wavelength [51]. The domain size that can be simulated thus scales with the amount of available computer memory along with the wavelength. The physics interface supports study types such as Eigenfrequency, Mode Analysis, Boundary Mode Analysis, and Frequency Domain, which is the focus of this thesis. The "Frequency Domain Study" type is used for

source driven simulations for a single frequency or sequence of frequencies [51]. Using this module, one end of the rectangular waveguide (shown in Figure 3.1 represented by air with respect to this thesis design) was assigned as Port 1 and the other end as Port 2 (also shown in Figure 3.1), where a TE_{10} electromagnetic signal of $10\,W$ was created to simulate the network analyzer's signal input. To obtain the correct resonant frequencies, the range of the study would need to be specified next.

3.2.2 Study

The "Frequency Domain Study" is used to compute the linear response or linearized model subjected to harmonic excitation for a single frequency or several frequencies [51]. The "Frequency Domain Study" accounts for the effects of all eigenmodes that are properly resolved by the mesh and how they couple with the applied loads or excitations [51]. The output of a "Frequency Domain Study" is typically displayed as a transfer function, magnitude or phase of deformation, sound pressure, impedance, or S-parameters versus frequency [51]. This research focuses on the last type of output. The "Frequency Domain Study" was configured to encapsulate the goal of obtaining the 10-GHz resonant frequency, namely the 9.5- to 10.5-GHz range, with a 100-kHz step size. This feature aided in narrowing down the exact resonant frequency of the empty cylindrical cavity, as will be shown shortly to equal 10.01 GHz and practically equal to the 10.0 GHz as originally intended. Another Study used was the Parametric Sweep, which helped model and simulate various rod sample radii, and disk sample radii and heights, as well as their permittivities. However, with the intent to measure material suitable for both infrared and microwave frequencies, the relative permittivity of focus will center around 10 +/- 1 between 8 and 10 GHz.

3.2.3 Building the Geometries

Instead of using arbitrary dimensions, the 10-GHz design for this thesis was emulated after a previous rectangular waveguide created by AFRL/RYHM, as previously shown in Chapter 2.4, but utilized a cylindrical cavity as opposed to a rectangular cavity. Equation 2.11 was utilized to solve for the required radius of the cylindrical cavity. The TM_{010} mode was chosen to design the cylindrical cavity following previous work suitable to the microwave region of research and for the high temperature consideration [13, 52, 35]. Solving for the radius, a, of the cylinder, Equation 2.11 was rewritten as

$$a = \frac{P_{nm}}{\sqrt{(\frac{f_0 2\pi\sqrt{\mu_r \epsilon_r}}{c})^2 - (\frac{l\pi}{h})^2}}[m], \tag{3.1}$$

where h is the height of the cavity and f_0 is the target empty cavity resonant frequency, which in the case of this research is 10 GHz. All other dimensions (i.e. height, length, and noting that the width referred to the diameter of the cylindrical cavity) were based off of the rectangular waveguide as previously described. This led to a being set equal to 1.1415 cm and shown in the top of Figure 3.1 as the modeled cavity. Cylinder geometries were used to create the internal cavity and coupling apertures of the design, while block geometries were used to create the waveguide and external cavity. After creating the geometry of the cavity, the geometries of the coupling apertures and rectangular waveguide were then designed. Rather than using an antenna-like coaxial cable to couple the waveguide to the cavity, apertures were used so that the coupling structure would not impede the path of the laser during heating. Additionally, a coupling structure can also change the resonant frequency of the empty cavity, which is another reason apertures were chosen to couple the waveguide to the cavity. The apertures were designed with a height, or thickness, of 0.1 cm, enabling the cavity walls to resemble realistic, physical dimensions. The radii

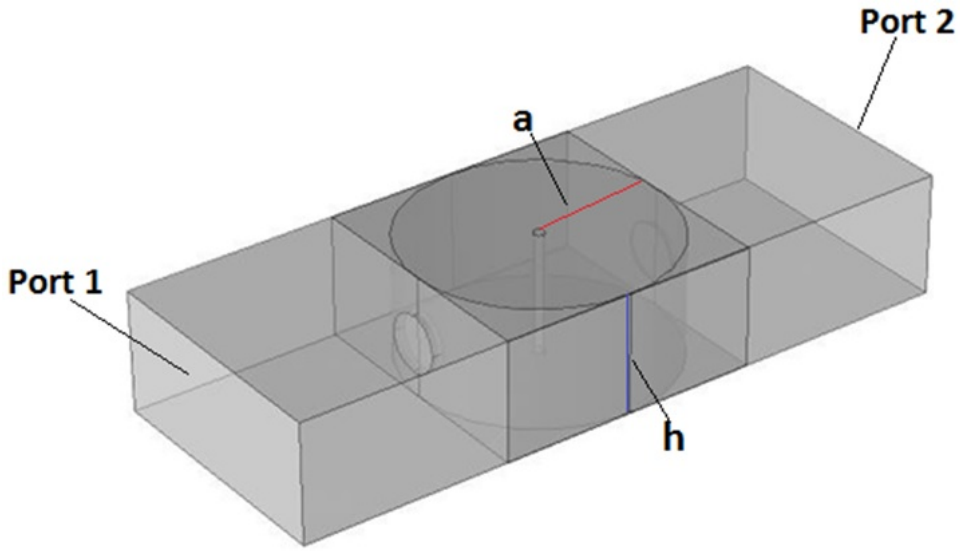

Figure 3.1. COMSOL Multiphysics® model of empty cylindrical cavity with Ports 1 and 2 labeled and where a and h is the radius and height of the cavity, respectively.

of the apertures were based on the "$b/2.2$" ASTM standard for rectangular waveguides and equated to $1.016\,cm/2.2$ or 4.618 mm [53]. This addition of the apertures can be seen in the middle of Figure 3.1. Finally, the rectangular waveguide itself was designed around both the cavity and the coupling apertures, as shown in the bottom of Figure 3.1.

With each component designed and modeled, every component of the design required an assignment of materials to be applied to them. This helped bridge the modeled design to the physical world by assigning real-world attributes to the design. Within the properties of the material, permittivity, as well as other properties, can be specified. The cylindrical cavity itself was assigned as copper and the rod and disk-shaped samples were assigned different permittivities, but with different radii, and heights in the case of the disk, in hopes of extracting which volumes produced the most sensitive changes with respect to resonant frequency. The apertures and inner dimensions of the rectangular waveguide of this design were each assigned as air to simulate the propagation of the electromagnetic signal towards, within, and through

the cylindrical cavity from Port 1 to Port 2.

3.2.4 Mesh

The "mesh" settings determine the resolution of the finite element mesh used to discretize the model [51]. The finite element method divides the model into small elements of geometrically simple shapes, which in this case were tetrahedrons [51]. This meshing was an important factor to the design as it enabled the physical representation of such a small model for a cylindrical cavity, as well as the even smaller rod- and disk-shaped samples. Too little meshing resulted in coarse S-Parameter peaks, while too fine of meshing led to extremely time-consuming computational simulations. Therefore, "finer-sized" mesh was chosen to proceed with for the simulations after considering the geometries to obtain a reasonable resolution balanced with realistic deadlines.

3.2.5 Simulation

The final step of simulating the design was to compute the "Studies", which would result in producing a model that depicts the design to include an electromagnetic field, as well as a plot with the S-Parameters, for an empty cavity. The former is shown in the top of Figure 3.2 and shows that the field is strongest at the center of the cylindrical cavity as expected [9]. The latter, shown in Figure 3.2 (bottom), depicted that an empty cavity's resonant frequency, with said dimensions, is 10.01 GHz for S_{21}. Note that if the magnitude of S_{21} is approximately equal to $0\,dB$, then there is little to no reflection of the signal. This magnitude can have better resolution with smaller step-sizes with respect to frequency during modeling.

Another check for the resonant frequency of the designed cylindrical cavity model was accomplished by Dr. Zahyun Ku, from AFRL/RXAN. By using CST, a 3-

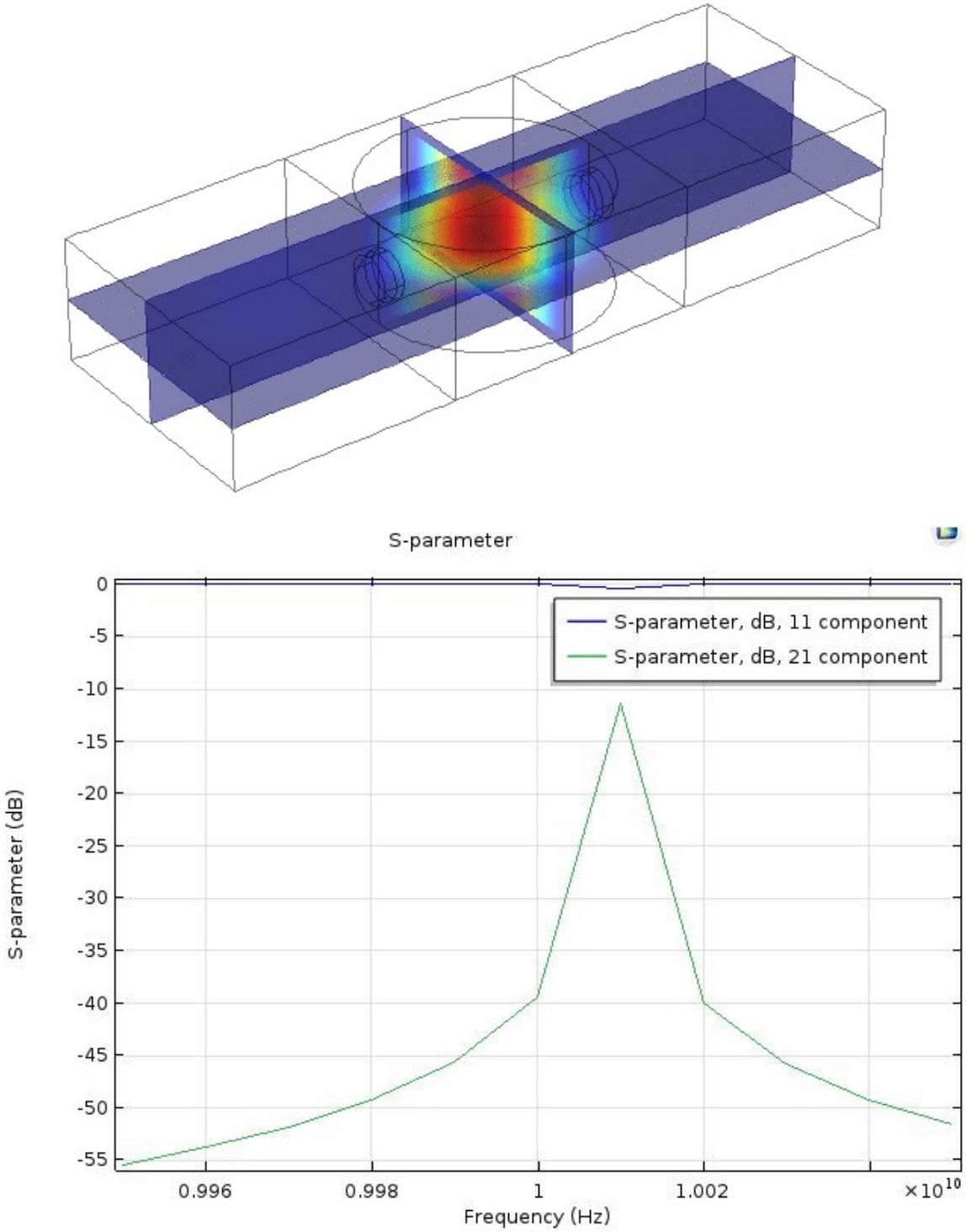

Figure 3.2. COMSOL Multiphysics® model of empty cylindrical cavity E-field (top); empty cylindrical cavity S-parameter (dB) at 10.01 GHz (bottom).

D electromagnetic simulation software, Figure 3.3 shows that, with the dimensions specified by this thesis' cylindrical model, the empty cavity resonates at 10.112 GHz. However, the diameter of the coupling aperture differs slightly as the CST model used a diameter of 0.6 mm, whereas this research uses 0.4618 mm calculated from the ASTM rectangular waveguide standard of $b/2.2$. Either way, due to the electric field strength at the center of the cavity, it is assumed that placing sample materials within the electric field at its maximum is the preferred location to correctly perturb the cylindrical cavity. With the empty cavity's resonant frequency established, the next step was to add a rod sample and measure its permittivity.

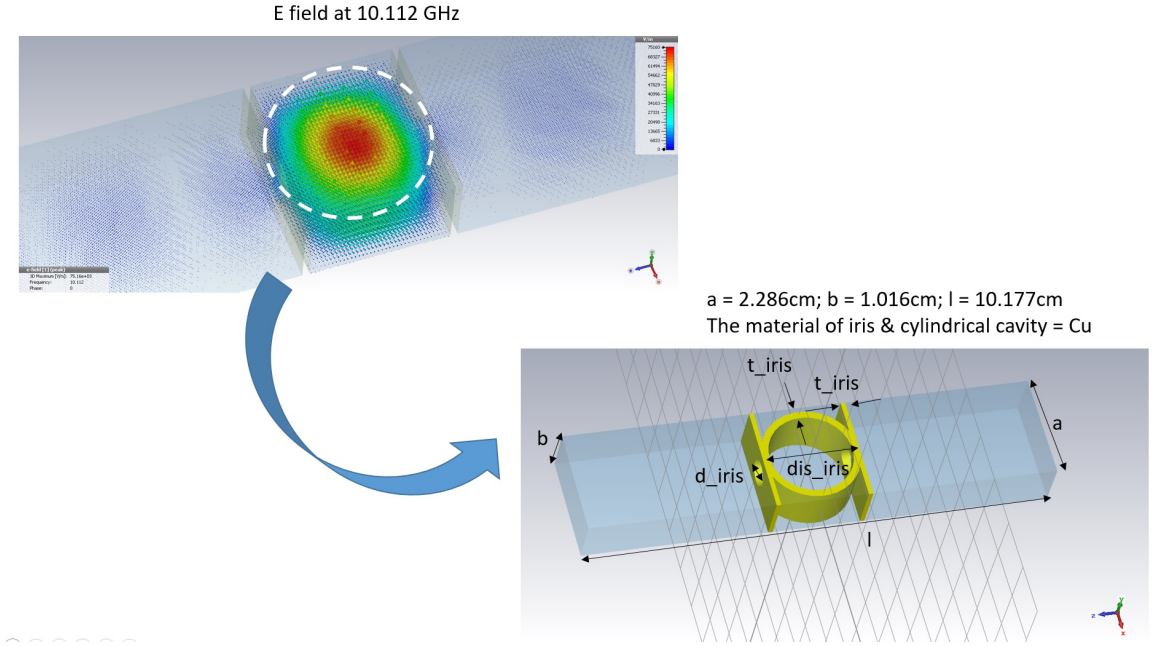

Figure 3.3. Computer Simulation Technology (CST) rendering of empty cylindrical cavity E-field resonating at 10.112 GHz used with permission.

3.2.5.1 Rod Sample

To test the accuracy of the designed cylindrical cavity, a FR-4 rod sample, whose empirical permittivity is known to equal 4.5, was tested first. Recall that the two basic assumptions of the approximation, Equation 2.12, were to ensure the change

in resonant frequency by introducing a material sample should be small compared to the resonant frequency of the empty cavity and that the sample's volume must be much smaller than the empty cavity's volume for Equation 2.12 to hold true [36]. The resonant frequency of the cylindrical cavity, with the rod sample with a 0.5mm radius, was 9.864 GHz. Given this resonant frequency, coupled with the empty cavity resonant frequency, and using Equation 2.12, the dielectric constant was calculated to be 4.34.

This permittivity is the true value of FR-4 with respect to the designed cylindrical cavity of this thesis within the confines of COMSOL Multiphysics®, but it indicates that Equation 2.12 is clearly an approximation and further refinement must be considered.

With these results being analyzed in the next chapter, the next step was to sweep various permittivities to determine if the model was sensitive enough to capture the frequency changes between temperature changes. The range of permittivities between 2.5 and 19.5 was swept in 1 MHz steps and the resulting S-Parameters are shown in the top and bottom of Figure 3.4, respectively 2.5 to 10.5 and 11.5 to 19.5, which does demonstrate that the modeled design can associate different permittivities with different perturbed resonant frequencies.

The Parametric Sweep was then configured to simulate various rod radii, ranging from 0.125mm to 1.2mm. Simultaneously, the permittivities of the rod sample were also to be swept at 9, 10, and 11, whose results and analysis will be shown in the next chapter.

These resonant frequencies could then be used to calculate the approximate dielectric constant, using Equation 2.12. This dielectric constant, being the real part of the complex permittivity, is the primary factor required to study the radome material and thus the focus of this thesis. However, one could find the imaginary factor, or

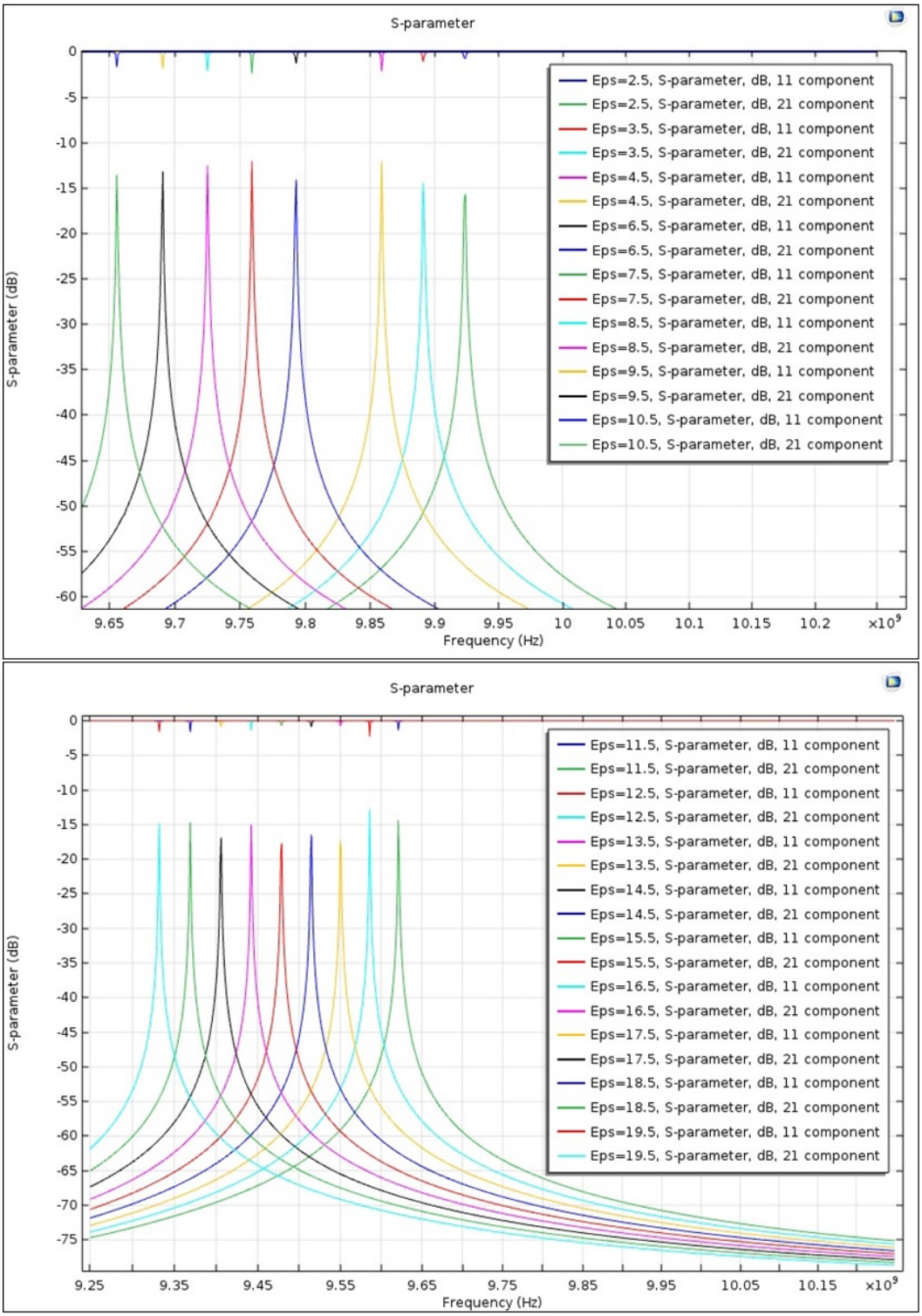

Figure 3.4. COMSOL Multiphysics® S-parameters plot of cylindrical cavity with FR-4 rod sample with 0.5 mm radius for Epsilon=2.5-10.5 sweep (top); cylindrical cavity with FR-4 rod sample with 0.5 mm radius for Epsilon=11.5-19.5 (bottom).

energy loss term, ϵ'', by first calculating the Q-factor by using Equation 2.14. Using the known variables for the rod sample thus far, the Q-factor for an empty cavity was 1,660.17, whereas it was 1,641.0 for a FR-4-perturbed cavity. Now with the Q-factors calculated, ϵ'' was found to be 0.0001, yielding the imaginary part as part of the complex permittivity, or $\epsilon^* = \epsilon' - j\epsilon''$. Knowing this also enables one to find the loss tangent, $tan\,\delta = \frac{\epsilon''}{\epsilon'}$, of known materials, resulting in a validation that the model provides approximated values as expected.

3.2.5.2 Disk Sample

With the model being able to obtain a close approximation of the desired permittivity, the sample was changed from a rod to a disk with the hopes of minimizing the temperature gradient when the sample is laser heated to simulate an extreme environment. This change meant that Equation 2.12 may or may not hold true as a viable approximation for finding the dielectric constant with disk samples. Instead, a new empirical approximation could be found from the data obtained by measuring the permittivities for a disk sample as followed.

Again, varying the permittivities in the Parametric Sweep properties from 9 to 11, a disk sample with a height of 150 μm was chosen by the research sponsors at AFRL due to the requirement of minimizing gradient heating in exchange for more uniform laser heating. Disk sample heights, or thicknesses, much greater than 150 μm would need to consider temperature gradients as a factor. Thus, a thin disk sample was preferred over a rod sample, which required a height equal to the cavity and results in a very noticeable temperature gradient if laser-heated from either end of the rod or any point in-between. Therefore, due to this requirement and relative sensitivity of the cavity structure, this thesis narrowed down the thickness of the disk sample to a height of 150 μm. However, other thicknesses, namely 75 μm and 225 μm, were

also considered in order to gauge the accuracy or error of the 150 μm height. On the other hand, the disk sample radius would also need to be considered, bearing in mind that the center of the cylindrical cavity contained the maximum strength of the electric field. It was shown that varying the radii for a disk sample yielded a different resonant frequency for each radius. Again, noting that the permittivities of interest for dual-spectrum materials were approximately 10, the range of 9 to 11 for permittivity was also used as a parameter for the disk sample to account for potential error centered around a dielectric constant of 10. The same simulation process for a disk sample was completed as previously stated for the rod sample, and those results will again be analyzed in the next chapter.

3.3 Summary

In this chapter, the cylindrical cavity was designed, modeled, and simulated to use the cavity perturbation technique for both rod and disk samples. The results from these simulations will now be revealed and analyzed, drawing conclusions to round out this thesis.

IV. Results and Analysis

4.1 Chapter Overview

To complete the research conducted by this thesis, the simulations accomplished in Chapter III needed to be post-processed. The results of these simulations are uncovered and analyzed for both the rod and disk samples. Finally, after the analysis, the fabricated design prototype and its initial findings will be discussed.

4.2 Results & Analysis

4.2.1 Rod Sample Results & Analysis

In order to analyze the results and compare them to theory, an analytic discussion must first be considered. Beginning with Equation 2.12, one can transform this linear equation into a quadratic function with the following derivation:

$$\epsilon' = 1 + 0.539 \times \frac{V_c(f_0 - f_s)}{V_s f_0} = 1 + 0.539 \times \frac{V_c}{V_s} - 0.539 \times \frac{V_c}{V_s}\frac{f_s}{f_0}, \tag{4.1}$$

where V_c and V_s equal $\pi h_c r_c^2$ and $\pi h_s r_s^2$, respectively, and h_c, h_s, r_c, and r_s are the heights and radii of the cavity and sample, denoted by the subscripts c and s, respectively.

$$\epsilon' = 1 + 0.539 \times (\frac{r_c}{r_s})^2 - 0.539 \times (\frac{r_c}{r_s})^2\frac{f_s}{f_0}, \tag{4.2}$$

This means that, in a general form,

$$\epsilon' = -c_1 f_s' + (1 + c_1), \tag{4.3}$$

which is linear with negative slope at this point, where c_1 equals $0.539 \times (\frac{r_c}{r_s})^2$ and

f_s' is $\frac{f_s}{f_0}$ called the normalized frequency. Combining V_c with 0.539 is called c_2 and solving for f_s' gives

$$f_s' = 1 - \frac{V_s(\epsilon' - 1)}{c_2}. \tag{4.4}$$

Similarly, the volumetric normalized frequency or, f_s'', which equals $\frac{f_s'}{V_s}$, can be found to be

$$f_s'' = \frac{1}{V_s} - \frac{\epsilon' - 1}{c_2}. \tag{4.5}$$

Rewriting Equations 4.4 and 4.5 results in

$$f_s' = 1 - c_3 {r_s}^2 \epsilon' + c_4, \tag{4.6}$$

where c_3 equals $\frac{\pi h}{c_2}$ and c_4 equals $\frac{V_c}{c_2}$ and

$$f_s'' = \frac{1}{\pi h_s r_s^2} - \frac{\epsilon' - 1}{c_2} = \frac{c_5}{r_s^2} - \frac{\epsilon' - 1}{c_2}, \tag{4.7}$$

where c_5 equals $\frac{1}{\pi h_s}$. Equations 4.6 and 4.7, plotted, can be analytically represented by Figure 4.1. Finally, taking the derivatives of Equations 4.6 and 4.7 with respect to the dielectric constant results in

$$\frac{df_s'}{d\epsilon'} = -c_3 r_s^2 \tag{4.8}$$

and

$$\frac{df_s''}{d\epsilon'} = -\frac{1}{c_2}, \tag{4.9}$$

respectively. With these equations, we see that the normalized frequency is a function of the sample radius, whereas the volumetric normalized frequency is a constant value related to the cavity volume.

As described in Chapter III and beginning with the rod sample, Figure 4.2 (d)

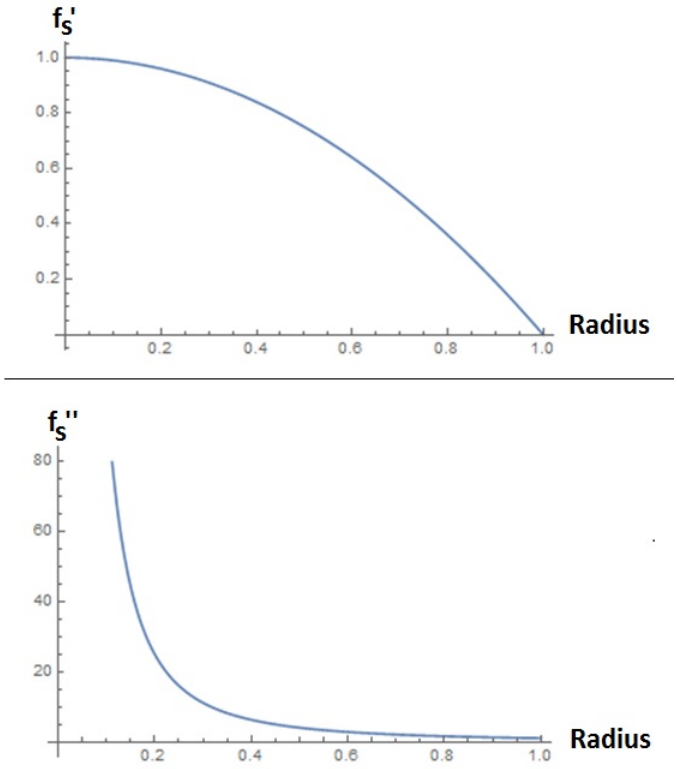

Figure 4.1. Analytical plot of f_s' (top) and f_s'' (bottom).

was plotted by sweeping the rod sample at a range of different radii and finding the normalized frequency at each radius, between the three different permittivities of 9, 10, and 11. This normalized frequency was found by dividing the resonant frequency by the empty cavity's resonant frequency of 10.01 GHz, shown as Equation 4.4. This resulted in a fairly quadratic fit, which agreed with the analytical approximation for normalized frequency, f_s', from Equation 4.6.

To determine the volume-dependence of the samples, a volumetric normalized frequency, f_s'', was considered during the analysis. Each rod sample volume was calculated for the various radii and was used to give the normalized frequency as a function of volume, or f_s'', then plotted in Figure 4.2 (c). This observed quadratic negative slope also agrees with the analytic function, Equation 4.7.

Another analysis conducted was to observe the constant from Equation 4.8. Figure

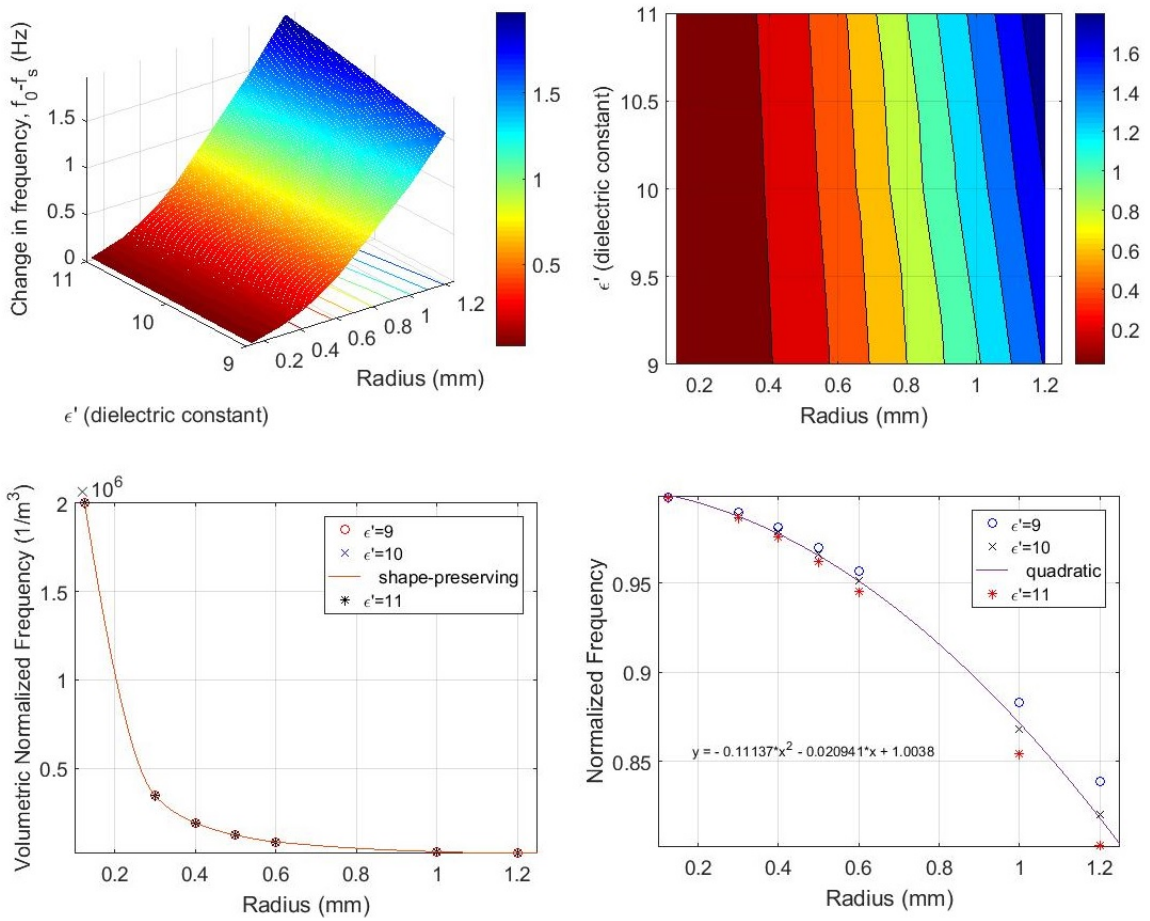

Figure 4.2. Rod sample plots: (a) shows that as radius and permittivity increases, so does $f_0 - f_s$; (b) similar to (a), but shows the "tilt" better; (c) Volumetric normalized frequency, f_s'', that shows similar negative curve of Figure 4.1 (bottom); (d) Normalized frequency, f_s', for the rod sample and the resulting quadratic fits for each permittivity (9, 10, and 11), ranging across each radii (0.3 mm, 0.4 mm, 0.5 mm, 0.6 mm, and 1 mm), which matches the top of Figure 4.1.

4.3 shows that von Hippel's approximation may not be valid for the study done here. The parabolic curve demonstrates that the larger the sample radius becomes, the further the data points get from the approximated constant of 0.539. However, as the radius of the sample increases to 1.15 mm, the constant begins to approach 0.539 once again.

Figure 4.2 (a) and (b) show that as the rod radius increases, the change in frequency also increases, which resulted in more sensitivity to observe the change in frequency between permittivities and agrees with Equation 4.8. However, coupling this information with Figure 4.2 (c) and (d) shows it may be best to use a 1.2-mm radius rod with balancing sensitivity ($f_0 - f_s$), volumetric normalized frequency (f_s''), and physically realistic dimensions in mind. At the 1.2-mm radius, there exists a well-defined separation between the permittivities, while ensuring the sample is well within the maximum of the electric field. Considering Figure 4.3, the von Hippel approximation could be modified as

$$\epsilon' = 1 + (0.162r_s^2 - 0.217r_s + 0.575)(\frac{r_c}{r_s})^2(1 - f_s'), \tag{4.10}$$

or

$$\epsilon' = 1 + (0.162 - \frac{0.217}{r_s} + \frac{0.575}{r_s^2})r_c^2(1 - f_s'). \tag{4.11}$$

Modifying Equations 4.8 and 4.9 to include the modified constant results in

$$\frac{df_s'}{d\epsilon'} = -\frac{r_s^2}{r_c^2(0.162r_s^2 - 0.217r_s + 0.575)} \tag{4.12}$$

and

$$\frac{df_s''}{d\epsilon'} = -\frac{1}{V_c(0.162r_s^2 - 0.217r_s + 0.575)}, \tag{4.13}$$

which are plotted in Figure 4.4 (left column). These plots show that $\frac{df_s'}{d\epsilon'}$ is a function

of the radius and $\frac{df_s''}{d\epsilon'}$ is effectively constant, which is fundamentally in agreement with Equations 4.8 and 4.9.

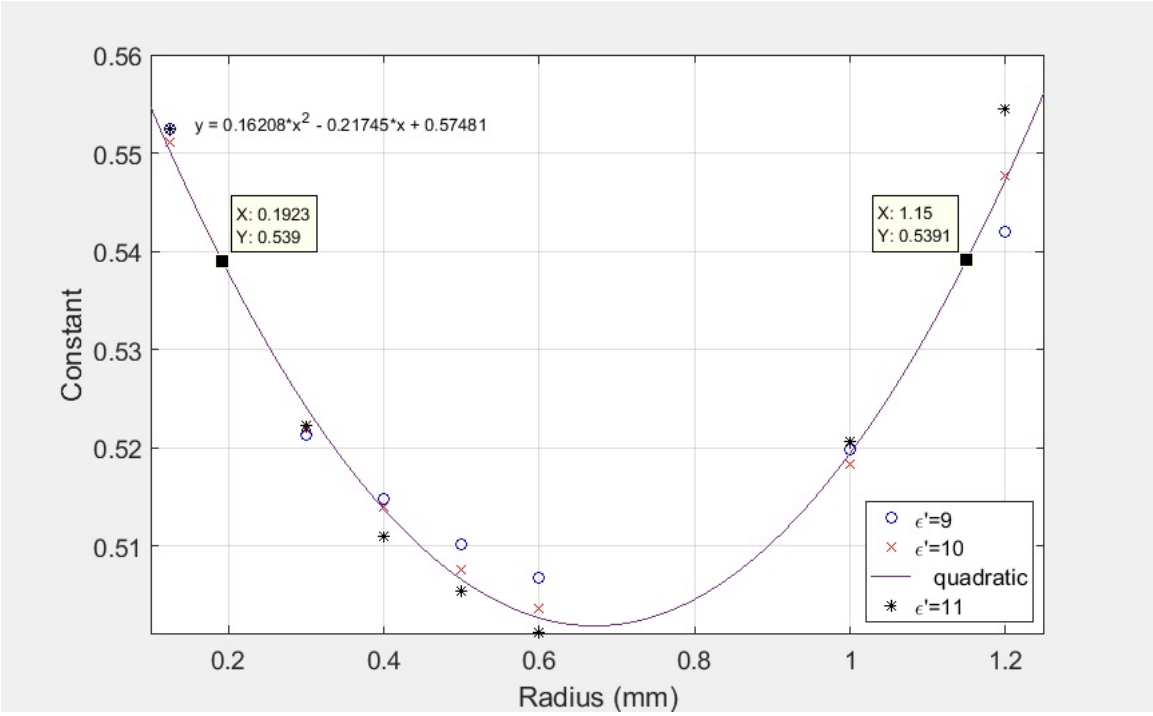

Figure 4.3. Rod sample plot shows quadratic curve of different c_2 constant for each radii that can be used to modify Equation 2.12.

4.2.2 Disk Sample Results & Analysis

With the rod sample simulations agreeing with the modified approximation, the disk sample results will now be analyzed to prove whether or not it also follows the approximation well or if a modified constant is also required. One difference between the rod and the disk samples is that the disk samples are not the same height of the cavity like the rod's height. More importantly is that the disk sample intercepts the cavity fields over a volume where the fields change significantly and cannot be assumed to be constant, as was von Hippel's assumption. As a reminder, a disk sample with a height of 150 μm was utilized in order to mitigate any temperature gradients during the laser heating experimentation. To understand the full extent of

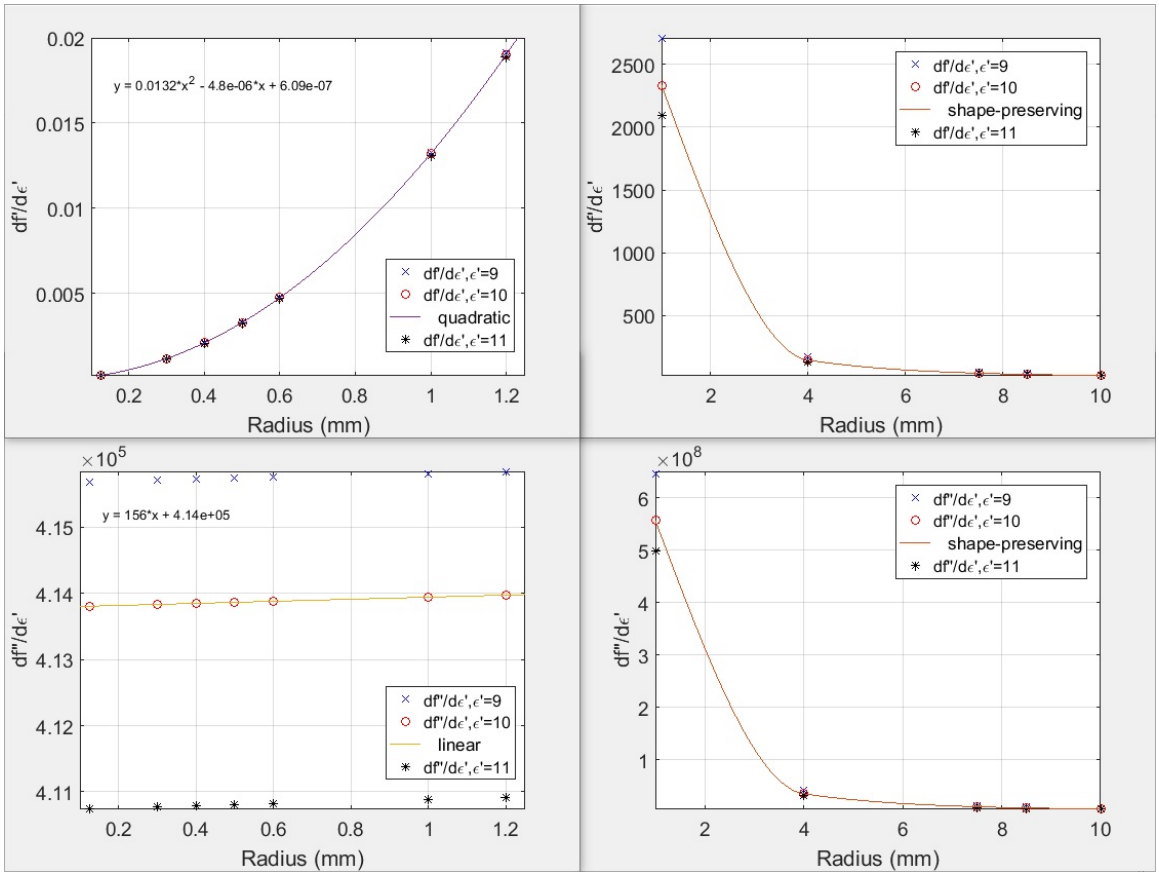

Figure 4.4. Rod sample plots of $\frac{df_s'}{d\epsilon'}$ that shows f_s' is only a function of the radius and $\frac{df_s''}{d\epsilon'}$ shows that f_s'' is a constant (left column); Disk sample plots of $\frac{df_s'}{d\epsilon'}$ and $\frac{df_s''}{d\epsilon'}$ that shows both f_s' and f_s'' are both functions of radius and ϵ' (right column).

having a disk height of 150 μm, additional data points were established to bolster the data set, namely by observing trends with disk heights of 75 μm and 225 μm as well. The 3-D and contour plots are shown in Figure 4.5, where the disk radii (1 mm, 4 mm, 7.5 mm, 8.5 mm, and 10 mm) are parametrically swept at the three different heights. Unlike the rod sample, the disk sample plots do not show much differentiation between the permittivities until the higher radii, around 7.5 mm (highlighted in red) are reached, signified by the tilting of the vertical gradient, thus providing better resolution between the permittivities. This tilting can be better observed in Figure 4.6. Thus the data suggests that for a very thin disk, 150 μm thickness in this case, the radii must have a large enough volume to observe a change in the resonant frequency between various permittivities.

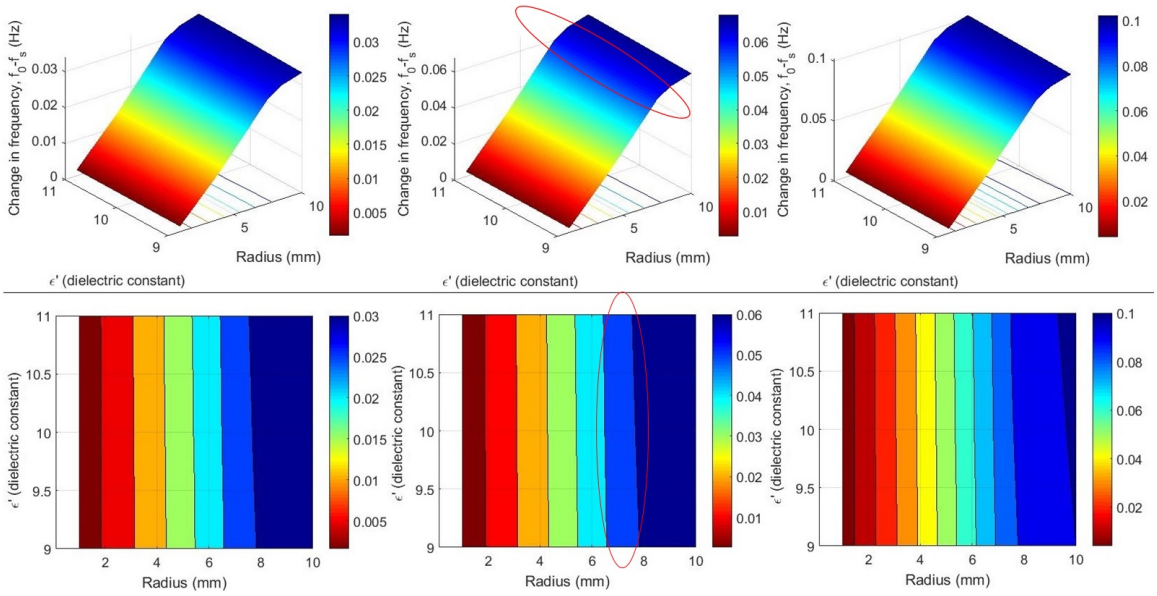

Figure 4.5. Disk sample plots that all show $f_0 - f_s$ is greater at the larger radii: 75 μm height (left column); 150 μm height (middle column); 225 μm height (right column). The color bars represent the change in frequency, or $f_0 - f_s$, in Hz.

On the other hand, similar to the rod samples, a similar volumetric dependency was seen and displayed in Figure 4.7 (bottom) and also matches the bottom of Figure 4.1. However, Figure 4.7 (top) shows a different functional form than that in Figure

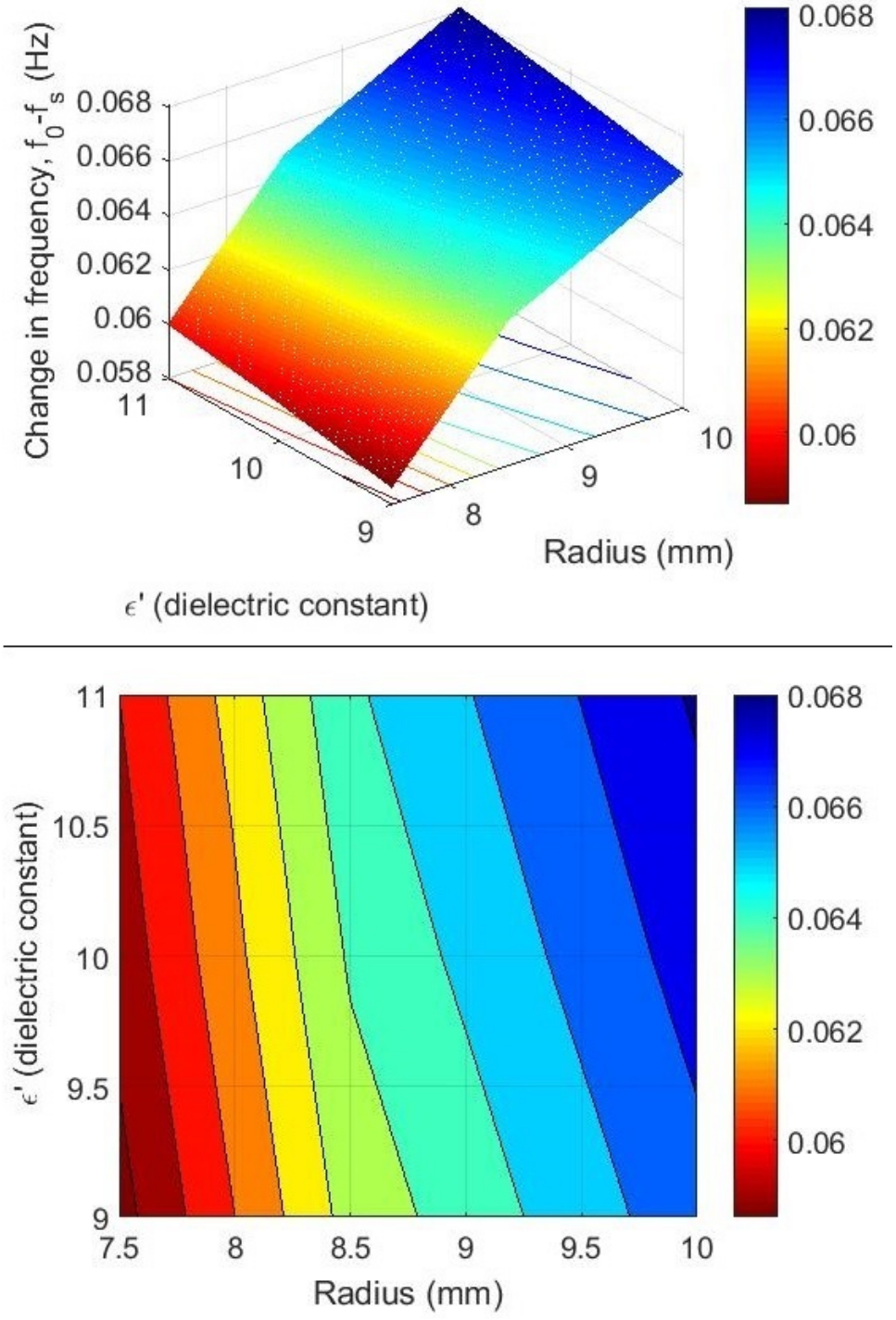

Figure 4.6. 150 μm height disk sample plot that shows greater change (tilt) between permittivities as the radius increases from 7.5mm to 10.0mm: 3-D plot (top); Contour plot (bottom). The color bars represent the change in frequency, or $f_0 - f_s$, in Hz.

4.1 (top), indicating the form of von Hippel's approximation is not appropriate for the disk samples. Similar to the rod data, the disk data at each height shows that there is an increase in the separation of the normalized frequency data (top of Figure 4.7), and thus permittivity, as radius is increased.

However, Figure 4.8, isolating the target of a 150 μm height disk, shows that the disk data constant is not 0.539 and is a function of the sample radius and also the permittivity. In other words, similar to the modified constant of the rod, the disk constant can be found using Figure 4.8, which will differ based on radii. The von Hippel approximation could again be modified for the disk as

$$\epsilon' = 1 + (0.113r_s^2 - 0.037r_s + 3.82)(\frac{V_c}{\pi r_s^2 h_s})(1 - f_s'), \tag{4.14}$$

or

$$\epsilon' = 1 + (0.113 - \frac{0.037}{r_s} + \frac{3.82}{r_s^2})\frac{V_c}{\pi h_s}(1 - f_s'). \tag{4.15}$$

Modifying Equations 4.8 and 4.9 to include the modified constant results in

$$\frac{df_s'}{d\epsilon'} = -\frac{r_s^2}{r_c^2(0.113r_s^2 - 0.37r_s + 3.82)} \tag{4.16}$$

and

$$\frac{df_s''}{d\epsilon'} = -\frac{1}{V_c(0.113r_s^2 - 0.37r_s + 3.82)}, \tag{4.17}$$

which are plotted in Figure 4.4 (right column). These disk sample plots show that both $\frac{df_s'}{d\epsilon'}$ and $\frac{df_s''}{d\epsilon'}$ are functions of radius and ϵ', which differs greatly from the results of the rod sample plots (Figure 4.4 (left column). They also show that the smaller the radius, the greater the sensitivity. However, even as the radius increases to larger radii, the sensitivity magnitude is much greater than that of the rod sample. With these promising results, we will now cover the fabrication of the design's prototype.

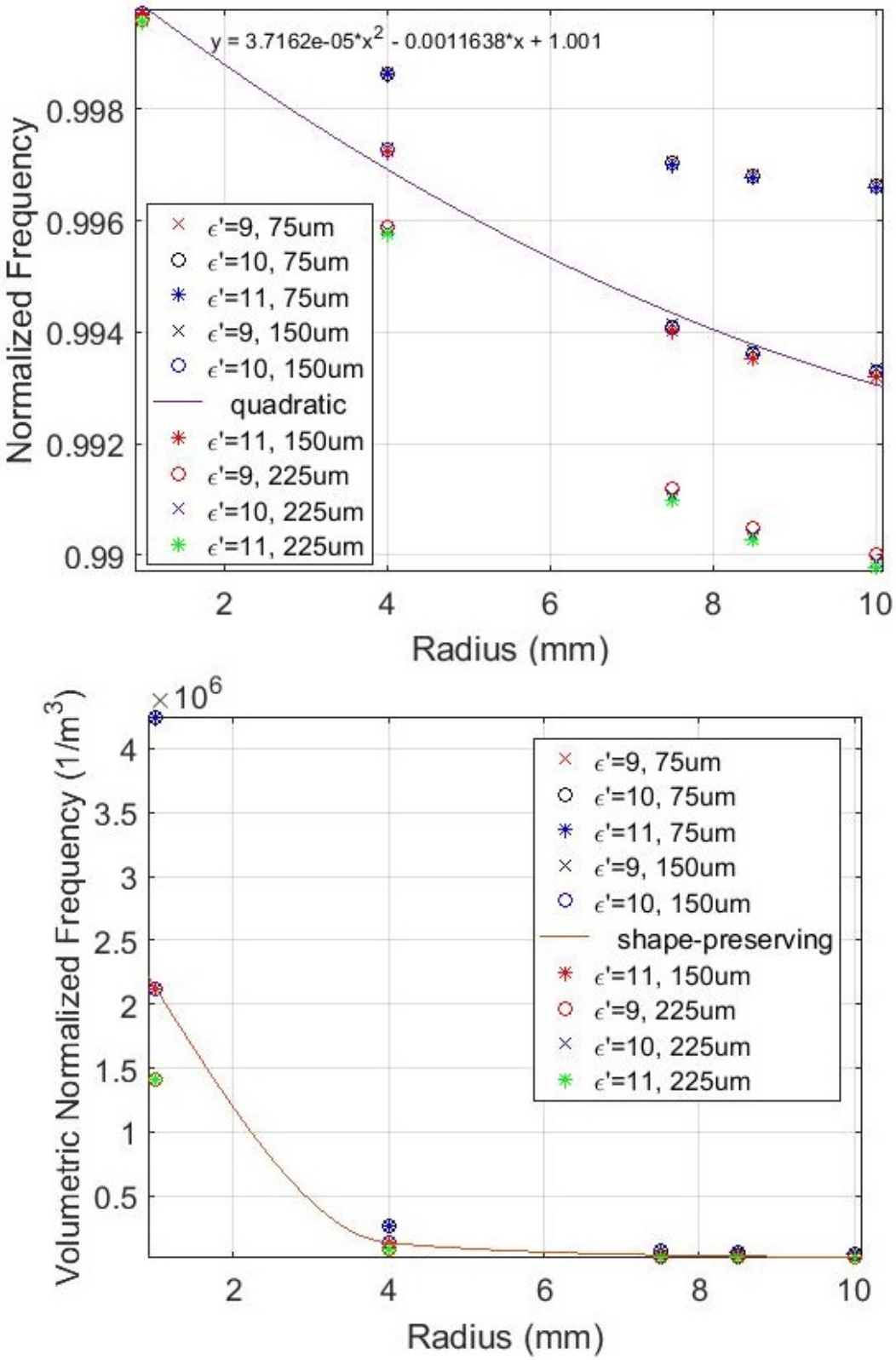

Figure 4.7. Normalized frequency, f_s', for disk heights of 75 μm, 150 μm, and 225 μm in radius (top); volumetric normalized frequency, f_s'' (bottom).

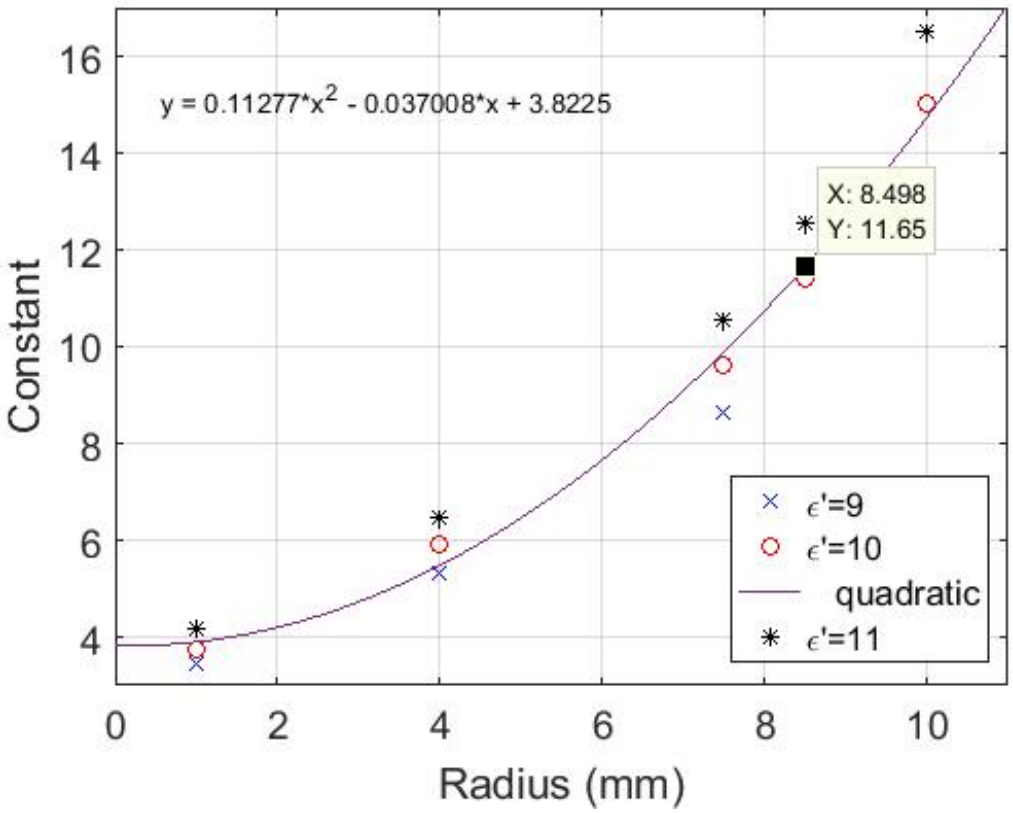

Figure 4.8. Disk sample plot shows quadratic curve of different c_2 constant for each radii that can be used to modify Equation 2.12.

4.3 Prototype

To begin transitioning the research into the experimental phase, the model was fabricated into a prototype, the top of Figure 4.9, with AFRL/RYHM's 3-D printer after exporting the COMSOL Multiphysics® design file as a CAD file. A view from the top as well as of the aperture are shown in the bottom and middle of Figure 4.9, respectively. However, the CAD engineers added a removable cavity topper in order to easily reposition or extract any misaligned samples. An external housing was also added to the model in order to connect the model to a network analyzer. Both of these additions are shown in Figure 4.10. The 3-D printed model was then metalized by the electroless copper deposition process shown in Figure 4.11. This electroless deposition of copper is a method of metallizing a polymer surface that does not require external applied voltages, vacuum equipment, or seed layers. Instead, deposition of copper occurs through a series of chemical reactions that are facilitated by a catalyst on the polymer surface. Deposition takes place in simple liquid baths, offering the possibility of batch processing for high throughput. These baths are less expensive than the equipment required for other deposition techniques such as the vacuum chambers required for sputter deposition [54].

The prototype was then fabricated, as shown in Figure 4.12, but initial testing of the resonant frequency for the empty cavity concluded that the metallization was not robust in some areas due to the lack of abrasion during fabrication. However, after creating a second prototype, AFRL/RYMH conducted initial experiments using two different rod samples to produce results that compared to the analytical approximation and the numerical modeling simulations provided by this thesis research. These results are shown in Figure 4.13, where the top shows the normalized S_{21} at its respective resonant frequency for an empty cavity, Vero White, and ALON [55], which matches the results of Figure 3.4. The bottom of Figure 4.13 shows the linear behav-

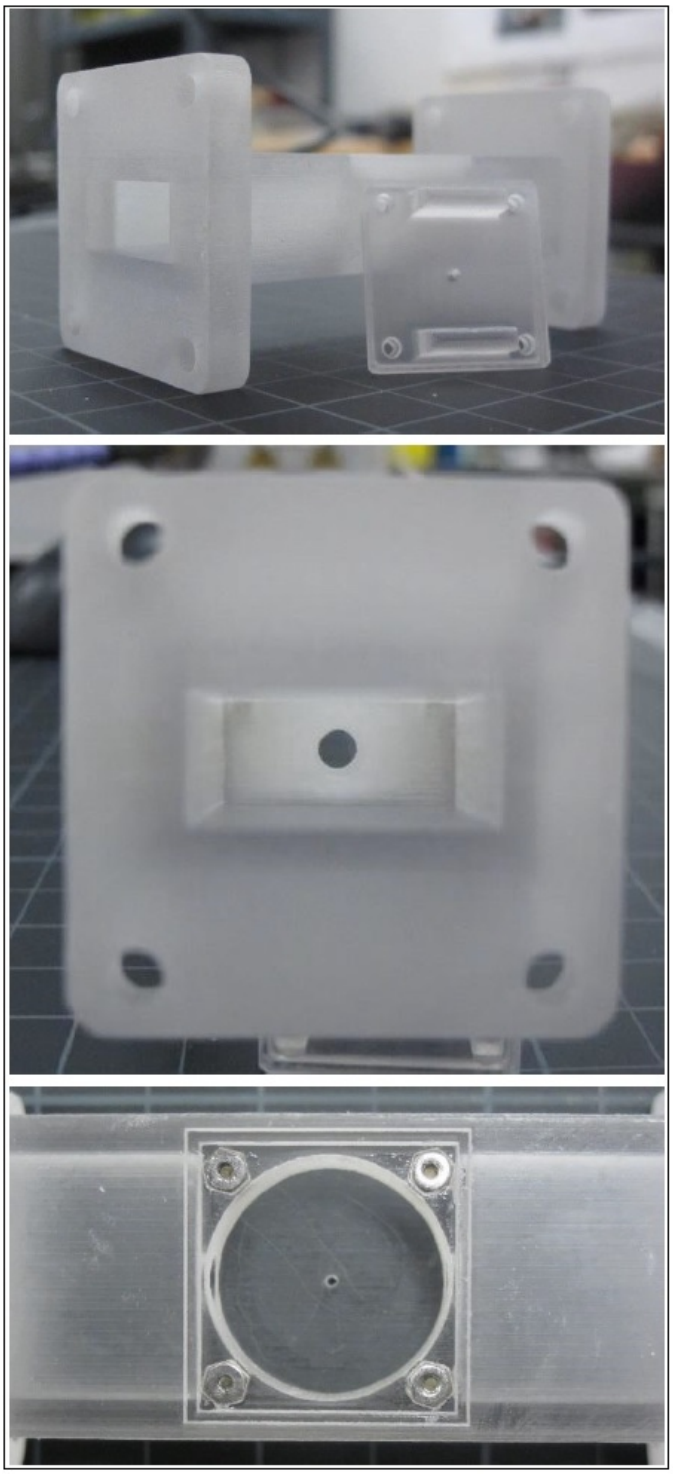

Figure 4.9. 3-D printed prototype of designed cylindrical cavity with removable top (top); internal cavity view of aperture (middle); top down view of cavity with rod sample hole (bottom).

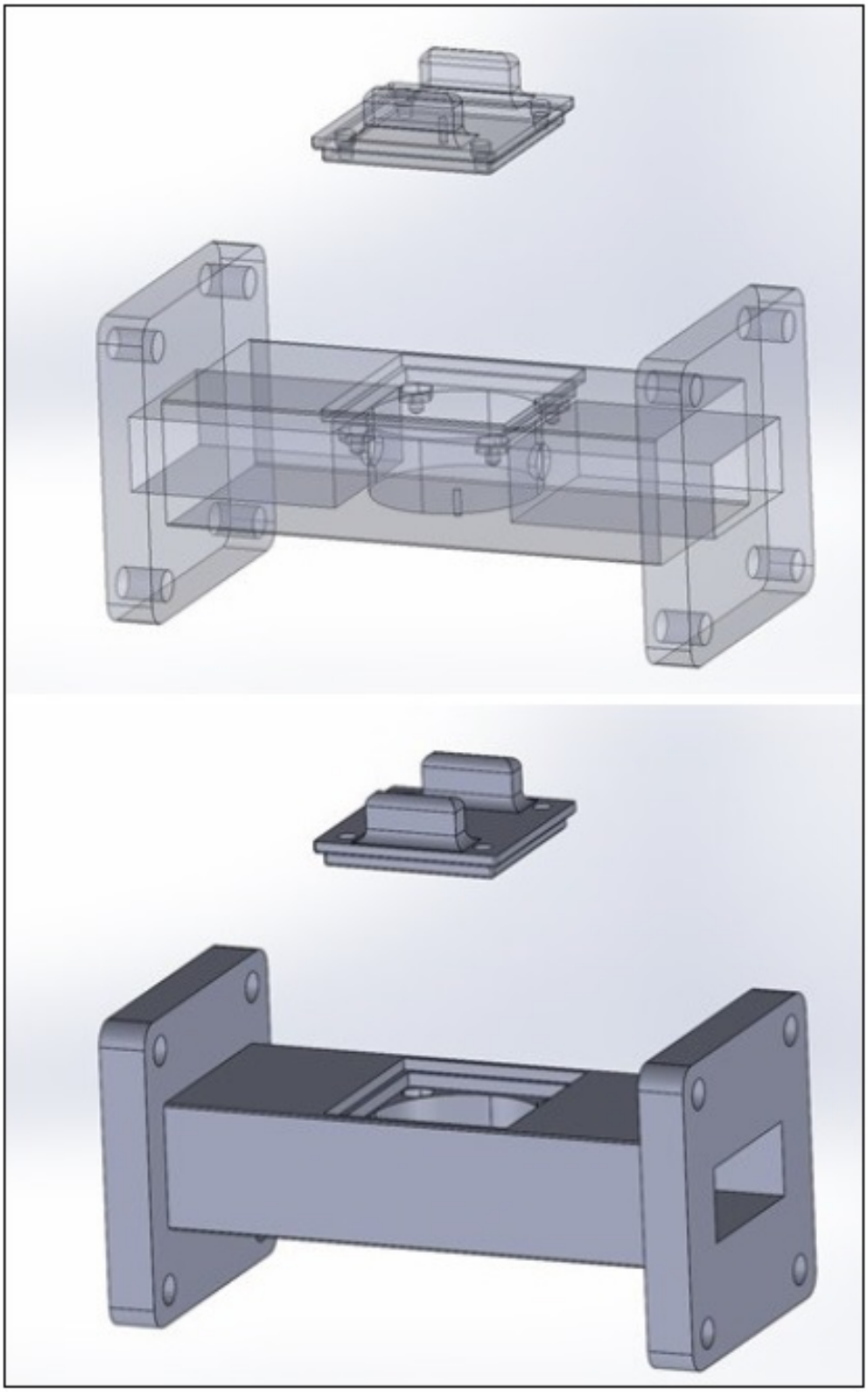

Figure 4.10. CAD modified rendering of the cylindrical cavity design within a rectangular waveguide and including the network analyzer flanges: removable top design (top); external housing (bottom).

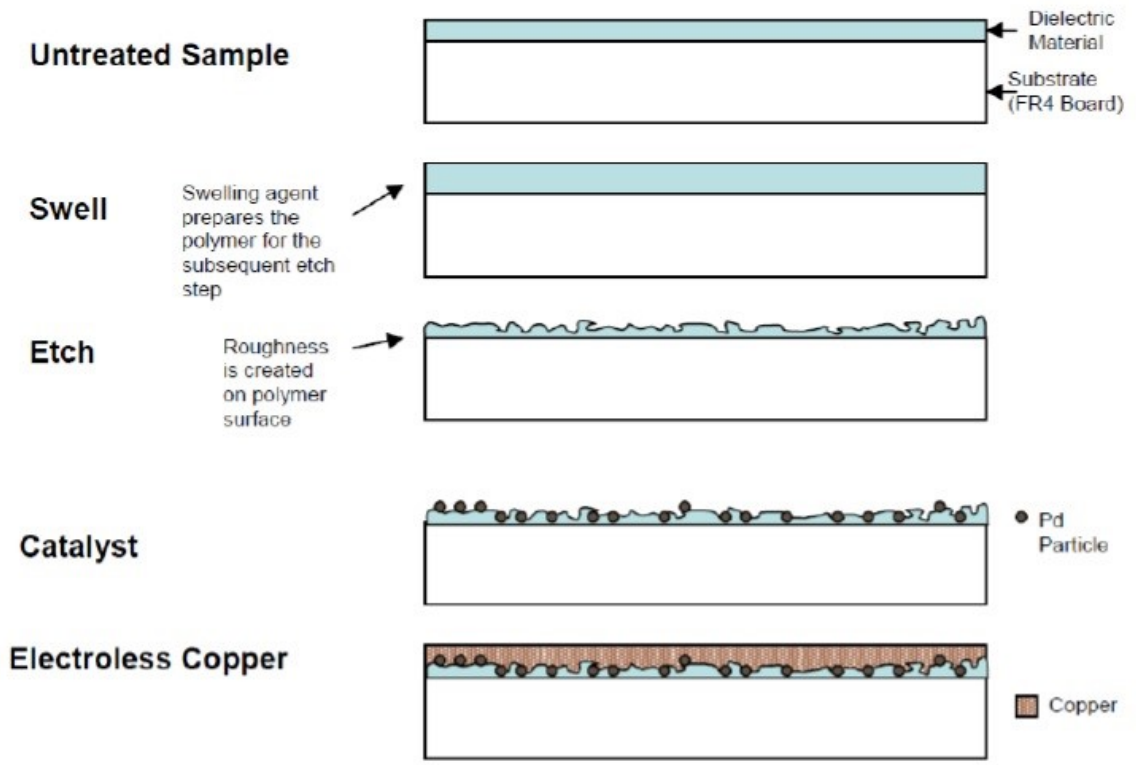

Figure 4.11. Electroless copper deposition process flow used to metallize 3-D printed prototype with copper.

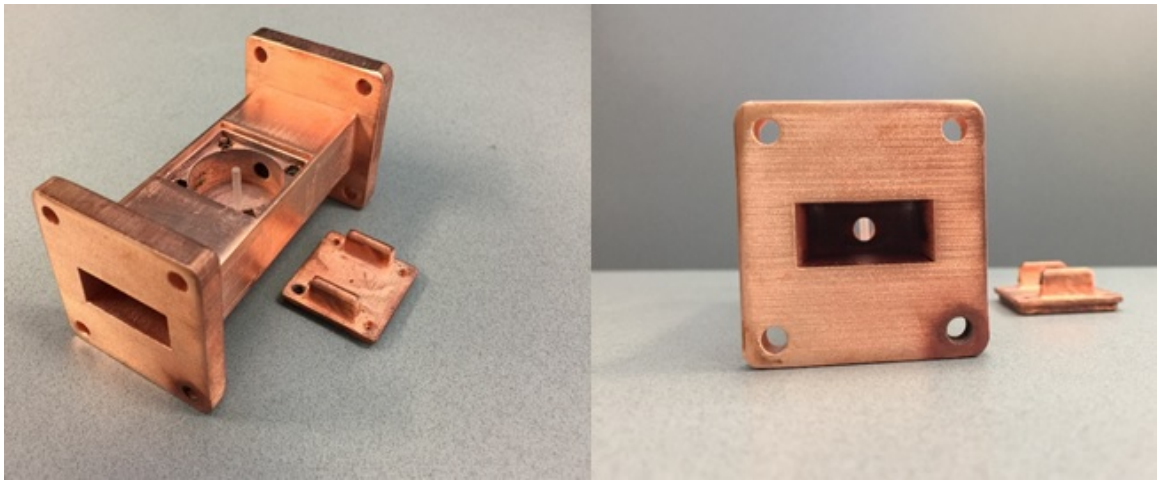

Figure 4.12. Copper deposited 3-D printed prototype of cylindrical cavity with removable top.

ior for the analytic approximation, numerical model simulations, and the empirical data from the prototype [55]. As shown, the change in frequency, $f_0 - f_s$, increases as permittivity increases, which agreed with the initial rod sample data shown in the top row of Figure 4.3.

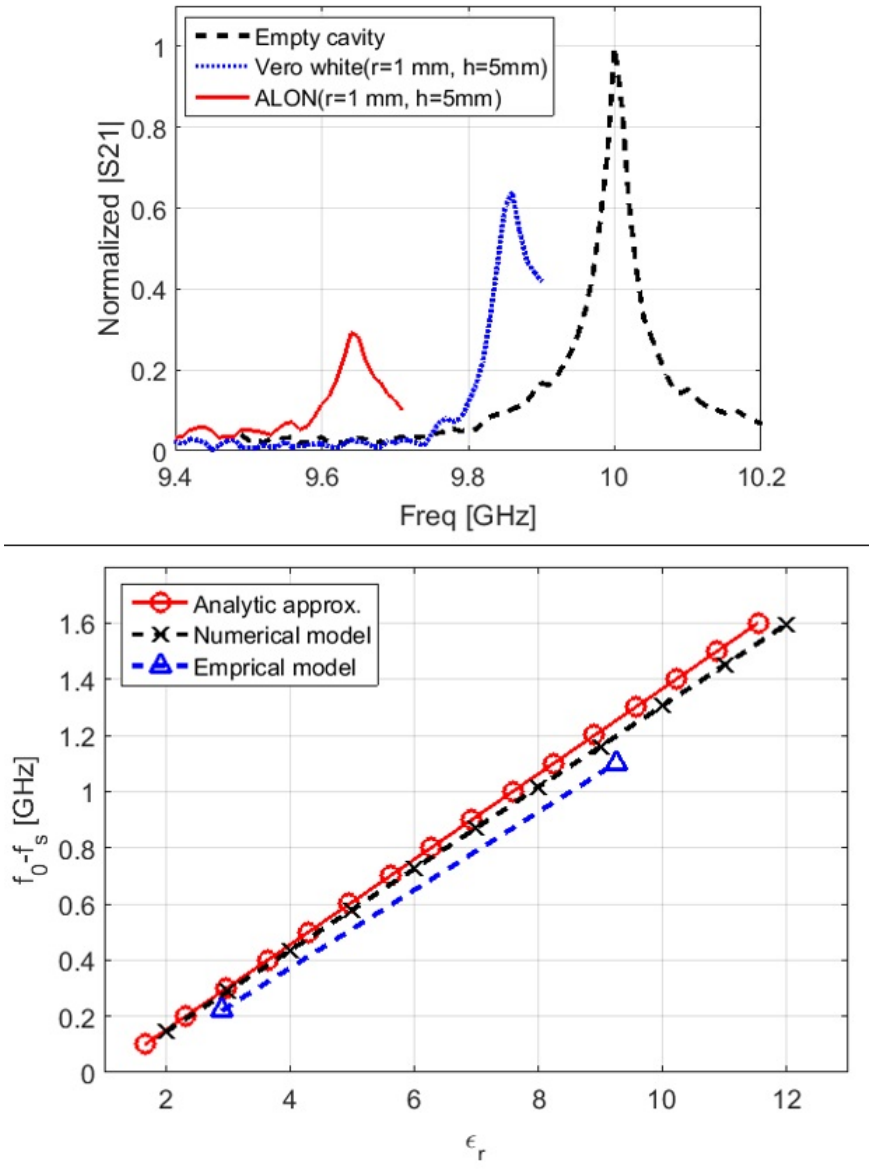

Figure 4.13. S_21 **for the empty cavity, Vero White, and ALON (top); linear comparison of analytic approximation, numerical model, and empirical data (bottom).**

4.4 Summary

As shown in this chapter, both the sample's shape and volume are important factors to consider when utilizing the cavity perturbation technique. The rod sample simulations followed von Hippel's functional form for calculating permittivity, but his constant must be replaced by a function of sample radius. Whereas the disk sample simulations showed that von Hippel's functional form is not appropriate for a disk. Keeping temperature gradient in mind, the disk sample could be used under laser-heating conditions to further progress the research of hypersonic vehicle windows/radomes as the change in cavity frequency as a function of permittivity should be sufficient to deduce change in permittivity as a function of change in temperature. Unfortunately, due to time constraints, this research was not able to simulate the laser heating of either sample shape and derive an expression for permittivity as a function of temperature, or $\epsilon(T)$. However, the model was able to demonstrate that it could work for such a task with additional research in the future. Nonetheless, with this demonstration, it is within the realm of the possible to achieve a permittivity-high-temperature correlation as in previous research, which concluded that as temperature increases, permittivities increase [13, 14].

V. Conclusions and Recommendations

5.1 Conclusions

After extensive simulations, this thesis design functioned as a 10 GHz cylindrical cavity, showing the cavity perturbation method could be utilized to measure the change in resonant frequency shift sensitive to temperature changes. In order to do so, the rod samples, with volumes much smaller than the cavity volume, were used to perturb the cavity and should not be larger in radius than 1.2 mm to ensure the sample remains within the confines of the maximum of the electric field while defining the separation between the permittivities, but must be the same length as the cavity height itself. Whereas, a disk sample used to perturb the cavity must have a small radius and a thickness, or height, of 150 μm, to observe optimum resonant frequency shift sensitivity, balanced with uniform heating capability, and also ensuring the disk is within maximum of the electric field. However, the sensitivity magnitude of the disk sample is so much greater than the rod sample that the radius can be between 6mm and 8 mm, while still maintaining that balance. In either case, the constant used in von Hippel's approximation, Equation 2.12, must be replaced by a quadratic function of sample radius for both rod and disk samples. Also, samples need to be placed in the center of the cavity where the maximum electric field exists. This research has shown that a more precise equation to calculate permittivity by measuring the resonant frequency shift could be extracted from the data obtained from the simulations. Nonetheless, the dielectric constant equation for a very small-radius rod sample, Equation 2.12, was used to initially design the model, but only holds true for samples with very small volumes. Although meshing is very important to consider during modeling, it was shown in the analysis that the sample's shape and volume are both critical pieces of the puzzle to obtain accurate dielectric property

measurements. In the end, this thesis designed a cylindrical cavity and utilized the cavity perturbation technique to analyze the measurement of the dielectric properties of radome materials, with the possibility to produce enough resonant frequency shift sensitivity at high temperatures.

5.2 Future Recommendations

Now that the model of this research has been validated to function as designed, there are extensive applications that it may be used for, but the following is recommended for future work:

1. Optimize the aperture size to achieve higher Q-factors for the cavity or S_{21} magnitudes at smaller step sizes (e.g. 1-10 MHz)

2. Incorporate laser heating physics to the current model to extract $\epsilon(T)$

3. Model A-sandwich dielectric materials for radome wall and simulate against laser-heated physics

4. Conduct experiments using a solid fabricated model to validate the design for known dielectric materials

Bibliography

[1] N. Khatavkar and K. Balasubramanian, "Composite materials for supersonic aircraft radomes with ameliorated radio frequency transmission-a review," *RSC Advances*, vol. 6, pp. 6709–6718, 2016.

[2] S. Walker *et al.*, "The darpa/af falcon program: The hypersonic technology vehicle 2 (htv-2) flight demonstration phase," *AIAA International Space Planes and Hypersonic Systems and Technologies Conference*, vol. 15th, pp. 1–9, 2008.

[3] R. Freedman *et al.*, *Universe*, 3rd ed. New York, NY: McGraw Hill, 2008.

[4] B. McGarry. Lockheed unveils plans for sr-72. defensetech.org. Defense Tech. [Online]. Available: https://defensetech.org/2013/11/04/lockheed-unveils-plans-for-sr-72/

[5] D. J. Kozakoff, *Analysis of Radome-Enclosed Antennas*, 2nd ed. Boston: Artech House, Inc., 1997.

[6] M. N. Data. The electromagnetic spectrum. nasa.gov. NASA. [Online]. Available: https://mynasadata.larc.nasa.gov/images/EM_Spectrum3-new.jpg

[7] H. Physics. Parallel plate with dielectric. gsu.edu. Hyper Physics. [Online]. Available: http://hyperphysics.phy-astr.gsu.edu/hbase/electric/dielec.html#c1

[8] M. Equations. Dielectric constant - permittivity. maxwells-equations.com. Maxwell's Equations. [Online]. Available: http://maxwells-equations.com/materials/permittivity.php

[9] D. Pozar, *"Microwave resonators," in Microwave Engineering*, 3rd ed. Hoboken, NJ: Wiley, 2005.

[10] K. Sasaki *et al.*, "Development of the complex permittivity measurement system for high-loss biological samples using the free space method in quasi-millimeter and millimeter wave bands," *Physics in Medicine and Biology*, vol. 58, pp. 1625–1634, 2013.

[11] J. Park and A. Urbas, "Electromagnetic and thermal design of optimal common aperture materials with ceramics and nano-composites," *Submitted to APRS*, vol. Spring Review, pp. 1–23, 2016.

[12] J. D. Walton, *"Design and Principles," in Radome Engineering Handbook*, 1st ed. New York, NY: Marcel Dekker, Inc., 1970.

[13] X. Ren *et al.*, "Characterization of sicn ceramic material dielectric properties at high temperatures for harsh environment sensing applications," *IEEE Transactions on Microwave Theory and Techniques*, vol. 61, pp. 960–971, 2013.

[14] N. D. Corbin, "Aluminum oxynitride spinel: A review," *Journal of European Ceramic Society*, vol. 5, pp. 143–154, 1989.

[15] F. Chen *et al.*, "Electromagnetic optimal design and preparation of broadband ceramic radome material with graded porous structure," *Progress in Electromagnetics Research*, vol. 105, pp. 445–461, 2010.

[16] J. Park and A. Urbas, "Electromagnetic and thermal design of optimal common aperture materials with ceramics and nano-composites," *Laboratory Research Initiation Request*, vol. Executive Summary, pp. 1–21, 2015.

[17] X. Li and Y. Jiang, "Design of a cylindrical cavity resonator for measurements of electrical properties of dielectric materials," Master's thesis, University of Gavle, Gvle, Sweden, 2010.

[18] J. Kirsch *et al.*, "Tri-mode seeker dome considerations," *Proceedings of SPIE - The International Society for Optical Engineering*, vol. 5786, pp. 33–40, 2005.

[19] D. E. Glass, "Ceramic matrix composite (cmc) thermal protection systems (tps) and hot structures for hypersonic vehicles," *AIAA International Space Planes and Hypersonic Systems and Technologies Conference*, vol. 2682, pp. 1–36, 2008.

[20] G. Russell *et al.*, "Army hypersonic compact kinetic energy missile laserwindow design," *Proceedings of SPIE - The International Society for Optical Engineering*, vol. 5078, pp. 1–13, 2003.

[21] A. Khan and R. Nema, "Analysis of five different dielectric substrates on microstrip patch antenna," *Internationl Journal of Computer Applications*, vol. 55, pp. 6–12, 2012.

[22] M. Skolnik, *Radar Handbook*, 9th ed. New York, NY: Clancy Marshall, 2011.

[23] G. A. E. Crone *et al.*, "Design and performance of airborne radomes: a review," *IEEE Proceedings*, vol. 128, pp. 451–464, 1981.

[24] L. M. Goldman *et al.*, "Dual ir/rf windows for laser communications," *Proceedings of SPIE*, vol. 8086, pp. A1–A14, 2009.

[25] U. Hingst and S. Krber, "Ir-window design for hypersonic missile seekers-thermal shock and cooling systems," *Proceedings of SPIE*, vol. 4369, pp. 662–672, 2001.

[26] T. Williams *et al.*, "An aerothermal flexible mode analysis of a hypersonic vehicle," *American Institute of Aeronautics and Astronautics*, vol. 331, 2006.

[27] J. L. Hesler *et al.*, "Thz vector network analyzer measurements and calibration," *21st International Symposium on Space Terahertz Technology*, vol. Oxford, pp. 318–320, 2010.

[28] B. Meng *et al.*, "Extended cavity perturbation technique to determine the comlex permittivity of dielectric materials," *IEEE Transactions on Microwave Theory and Techniques*, vol. 43, pp. 2633–2636, 1995.

[29] V. V. Varadan *et al.*, "Free-space, broadband measurements of high-temperature, complex dielectric properties at microwave frequencies," *IEEE Transactions on Instrumentation and Measurement*, vol. 40, pp. 842–846, 1991.

[30] A. W. Kraszewski, "Observations on resonant cavity perturbation by dielectric objects," *IEEE Transactions on Microwave Theory and Techniques*, vol. 40, pp. 151–155, 1992.

[31] C. A. Balanis, *"Circular cross-section waveguides and cavities," in Advanced Engineering Electromagnetics*, 1st ed. New York, NY: Wiley, 1989.

[32] C. G. Montgomery, *"The measurement of dielectric constants," in Technique of Microwave Measurements*, 2nd ed. New York, NY: Dover Publications, Inc., 1966.

[33] M. S. Venkatesh and G. S. V. Raghavan, "An overview of dielectric properties measuring techniques," *Canadian Biosystems Engineering/Le genie des biosystemes au Canada*, vol. 47, pp. 7.15–7.30, 2005.

[34] O. Klein *et al.*, "Microwave cavity perturbation technique: Part i: Principles," *International Journal of Infrared and Millimeter Waves*, vol. 14, pp. 2423–2456, 1993.

[35] J. M. Catala-Civera *et al.*, "Dynamic measurement of dielectric properties of materials at high temperature during microwave heating in a dual mode cylindrical cavity," *Rev. Sci. Instrum.*, vol. 66, pp. 1070–1071, 1995.

[36] A. von Hippel, *"Dielectric Measuring Techniques," in Dielectric Materials and Applications*, 1st ed. Cambridge, MA: Technology Press of MIT, 1954.

[37] R. G. Carter, "Accuracy of microwave cavity perturbation measurements," *IEEE Transactions on Microwave Theory and Techniques*, vol. 49, pp. 918–923, 2001.

[38] R. A. Waldron, "Perturbation theory of resonant cavities," *IEEE Monograph*, vol. 373, pp. 272–274, 1960.

[39] A. D. Vyas *et al.*, "Cavity perturbation technique for complex permittivity measurement of dielectric materials at x-band microwave frequency," *Proceedings of International Conference on Microwave*, vol. 08, pp. 836–838, 2008.

[40] S. B. Cohn and K. C. Kelly, "Microwave measurement of high-dielectric constant materials," *IEEE Transactions on Microwave Theory and Techniques*, vol. MTT-14, pp. 406–410, 1966.

[41] A. Parkash *et al.*, "Measurement of dielectric parameters at microwave frequencies by cavity-perturbation technique," *IEEE Transactions on Microwave Theory and Techniques*, vol. MTT-27, pp. 791–795, 1979.

[42] L. Hartshorn and W. H. Ward, "The measurement of the permittivity and power factor of dielectrics at frequencies from 10^4 to 10^8 sycles per second," *Journal IEEE*, vol. 79, pp. 597–609, 1936.

[43] M. G. Broadhurst and A. J. Bur, "Two-terminal dielectric measurements up to 6×10^8," *Journal of Research of the National Bureau of Standards*, vol. 69C, pp. 165–172, 1965.

[44] K. J. Bois *et al.*, "Two-terminal dielectric measurements up to 6×10^8," *IEEE Transactions of Instrumentation and Measurement*, vol. 48, pp. 1141–148, 1999.

[45] S. Dudorov *et al.*, "Open resonator technique for measurement of thin dielectric film properties on optically dense substrates," *Materials Research Society Symposium*, vol. AA, pp. 1.7.1–.1.7.6, 2000.

[46] Y. Gui and W. Dou, "Open resonator technique of non-planar dielectric objects at millimeter wavelengths," *Progress In Electromagnetics Research M*, vol. 9, pp. 185–197, 2009.

[47] T. M. Hirvonen *et al.*, "Measurement of dielectrics at 100 ghz with an open resonator connected to a network analyzer," *IEEE Transactions of Instrumentation and Measurement*, vol. 45, pp. 780–786, 1996.

[48] W. W. Ho, "High temperature millimeter wave dielectric characterization of radome materials," *Proceedings SPIE*, vol. 362, pp. 190–195, 1983.

[49] R. J. Cook and C. B. Rosenberg, "Measurement of the complex refractive index of isotropic and anisotropic materials at 35 ghz using a free space microwave bridge," *Journal of Physics D: Applied Physics*, vol. 12, pp. 1643–1652, 1979.

[50] J. Kouroupis, "Flight capabilities of high-speed-missile radome materials," *John Hopkins APL Technical Digest*, vol. 13, pp. 386–392, 1992.

[51] *COMSOL Multiphysics® version 5.2a*, COMSOL Group, "www.comsol.com", 2017.

[52] B. Meng *et al.*, "A system to measure complex permittivity of low loss ceramics at microwaves frequencies and over large temperatures," *Rev. Sci. Instrum.*, vol. 66, pp. 1070–1071, 1995.

[53] *ASTM Standard D2520*, American Society for Testing and Materials, 2013.

[54] H. T. Hayden, "Enhanced adhesion between electroless copper and advanced substrates," Ph.D. dissertation, Georgia Institute of Technology, Atlanta, GA, 2008.

[55] J. Park *et al.*, "High temperature materials characterization for multispectral window applications," *SPIE DCS Defense+ Conference*, vol. 10179, pp. 1–8, 2017.

REPORT DOCUMENTATION PAGE

Form Approved
OMB No. 0704–0188

1. REPORT DATE *(DD–MM–YYYY)*	2. REPORT TYPE	3. DATES COVERED *(From — To)*
23 Mar 2017	Master's Thesis	May 2015 — 23 March 2017

4. TITLE AND SUBTITLE

Cavity perturbation technique of 10 GHz cylindrical resonator for modeling RF/IR sensor radomes/windows

5a. CONTRACT NUMBER

5b. GRANT NUMBER

5c. PROGRAM ELEMENT NUMBER

6. AUTHOR(S)

Arida, Marvin-Ray, Captain

5d. PROJECT NUMBER

5e. TASK NUMBER

5f. WORK UNIT NUMBER

7. PERFORMING ORGANIZATION NAME(S) AND ADDRESS(ES)

Air Force Institute of Technology
Graduate School of Engineering and Management (AFIT/EN)
2950 Hobson Way
WPAFB OH 45433-7765

8. PERFORMING ORGANIZATION REPORT NUMBER

AFIT-ENP-MS-17-M-086

9. SPONSORING / MONITORING AGENCY NAME(S) AND ADDRESS(ES)

AFRL/RXAN
Att: Dr. Augustine Urbas
2977 Hobson Way
WPAFB OH 45433
Email: augustine.urbas@us.af.mil

10. SPONSOR/MONITOR'S ACRONYM(S)

AFRL/RX

11. SPONSOR/MONITOR'S REPORT NUMBER(S)

12. DISTRIBUTION / AVAILABILITY STATEMENT

DISTRIBUTION STATEMENT A:
APPROVED FOR PUBLIC RELEASE; DISTRIBUTION UNLIMITED.

13. SUPPLEMENTARY NOTES

14. ABSTRACT

Dielectric properties of candidate materials for hypersonic vehicle radomes, which can reach above 1,500° Celsius, are required. Although there has been recent study for temperature dependence of dielectric constants, little is known near or above 1,500° Celsius. Current research uses laboratory-sized furnaces to achieve these temperatures, but this also requires large-sized and expensive samples. To reduce these costs, this thesis modeled a rectangular waveguide aperture-coupled to a 1.016cm-height, 1.1415cm-radius cylindrical cavity designed to operate at a resonant frequency of 10GHz. It utilized the electromagnetic cavity-perturbation method to optimize the research of small dielectric disk samples. The objective was to model a much smaller system, produce an empirical relationship between cavity resonance and the sample's dielectric constant, and create a prototype of the design to validate this concept. It was found that a disk of 150 μm thickness and small radius, positioned at the center of the cavity, is a viable geometry to produce sensitivity required to conduct dielectric measurements as a function of temperature. —Marvin-Ray Arida, Capt, USAF

15. SUBJECT TERMS

dielectric constant, permittivity, cavity perturbation method, cylindrical cavity resonator, hypersonic, radome

16. SECURITY CLASSIFICATION OF:			17. LIMITATION OF ABSTRACT	18. NUMBER OF PAGES	19a. NAME OF RESPONSIBLE PERSON
a. REPORT	b. ABSTRACT	c. THIS PAGE			Dr. M. Marciniak, AFIT/ENP
U	U	U	UU	84	19b. TELEPHONE NUMBER *(include area code)* (937) 255-3636, x4529; mmarcini@afit.edu